Ecological Complexity 29 (2017) 10–29

Contents lists available at ScienceDirect

Ecological Complexity

journal homepage: www.elsevier.com/locate/ecocom

Original Research Article

On ecosystems dynamics

M. Stehlík [a,b,*], P. Aguirre [c], S. Girard [d], P. Jordanova [e], J. Kiseľák [f], S. Torres [c], Z. Sadovský [g], A. Rivera [h,i]

[a] Department of Applied Statistics, Johannes Kepler University in Linz, Austria
[b] Institute of Statistics, University of Valparaíso, Gran Bretaña 1111, Valparaíso, Chile
[c] Departamento de Matemática, Universidad Técnica Federico Santa María, Casilla 110-V, Valparaíso, Chile
[d] Inria Grenoble Rhône-Alpes, France
[e] Department of Mathematic and Informatics, Shumen University, Shumen, Bulgaria
[f] Institute of Mathematics, P.J. Šafárik Univesity in Košice, Slovakia
[g] Independent Researcher formerly Institute of Construction and Architecture of the Slovak Academy of Science, Bratislava, Slovakia
[h] Laboratorio de Glaciología, Centro de Estudios Científicos, Arturo Prat 514, Valdivia, Chile
[i] Departamento de Geografía, Universidad de Chile, Marcoleta 250, Santiago, Chile

ARTICLE INFO

Article history:
Received 15 July 2016
Received in revised form 7 November 2016
Accepted 9 November 2016
Available online 29 November 2016

Keywords:
Stochasticity
Determinism
Chaos
Autonomous system
Guanaco glacier
Snow extremes

ABSTRACT

We show how a dynamical system given by a t-score function for some class of monotonic data transformations generates consistent extreme value estimators. The variation of their values increases the uncertainty of proper assessment of climate change. Two important examples illustrate the methodology: mass balance measurements on Guanaco glacier, Chile, and extreme snow loads in Slovakia. We experience singular learning of the transitions in ecosystems.

1. Introduction

In the past several decades scientific effort has been focused on studying and understanding global climate changes. The effect of climatic changes has become more and more visible and in many regions of the world these changes are represented by increasing of weather extremes (Chan et al., 1873; Coumou and Rahmstorf, 2012; Klein Tank and Können, 2003).

All ecosystems (Methan (Sabolova et al., 2015), Guanaco Glacier (Jordanova et al., 2016), Snow extremes (Stehlík et al., 2015)) are oscillating. Decomposition to deterministic, stochastic and chaotic part have been studied by Stehlík et al. (2016). We can understand contributions to oscillations in at least three following ways:

(1) Extreme Value Index (EVI) ξ oscillates around 0 (it can have positive, negative or zero values). As Penalva et al. (2016) pointed out, difficulties may rise with the "Regularity conditions" for the maximum likelihood (ML) estimation (Smith, 1985), it is shown that the usual property of asymptotic normality holds provided the extreme value parameter ξ is larger than -0.5. For all environments we can consider $\xi > -1$ (Penalva et al., 2016). Recently, Zhou (2009, 2010) showed that the ML estimators verify the property of asymptotic normality for $\xi > -1$. The Second Order Regularity condition (SOC) can be difficult to be checked (or even satisfied) in practical application. E.g. if the observed random variable (r.v.) is a power of Uniform or has power law behavior at the finite right end point (see Example 3.3.15 and 3.3.16, page 137, Embrechts et al., 1987), there is not unique SOC parameter ρ.

* Corresponding author at: University of Valparaíso, Gran Bretaña 1111, Valparaíso, Chile.
E-mail addresses: Milan.Stehlik@jku.at (M. Stehlík), pablo.aguirre@usm.cl (P. Aguirre), Stephane.Girard@inria.fr (S. Girard), pavlina_kj@abv.bg (P. Jordanova), jozef.kiselak@upjs.sk (J. Kiseľák), sebastian.torresle@alumnos.usm.cl (S. Torres), zoltan@sadovsky.info (Z. Sadovský), arivera@cecs.cl (A. Rivera).

http://dx.doi.org/10.1016/j.ecocom.2016.11.002
1476-945X/

(2) Aside of (1), the consistent estimators of tail parameters can be built up upon t-scores (Jordanova et al., 2016). The parameters of harmonic mean estimators (HME) are consisting dynamical system which can surprisingly always find a monotonic representing data function (t-score function) η. This process contributes to deterministic dynamics of Stehlík et al. (2016).
(3) The use of Negative t-Hill(n-t-Hill) for estimation of the EVI index $\xi < 0$) can give several limiting behaviors, however, limits can be given by symmetric (normal) or classical (Weibull) distributions, which both are special cases of generalized gamma distribution (ggd), see Stehlík (2008).

The paper is organized as follows. In the next session we study autonomous system of t-score functions. In Section 3 we study mass balance measurements from Guanaco glacier and we show that both negative and positive EVIs are obtained. In Section 4 we study the extremal snow loads in Slovakia, again receiving both negative and positive EVIs. To maintain the readability of the manuscript we put technicalities to Appendix.

2. Dynamical systems of t-score functions

The transformation-based score (Fabián, 2001; Stehlík et al., 2010) or shortly the t-score for the density f is defined as

$$T_\eta(x;\theta) = -\frac{1}{f(x;\theta)}\frac{d}{dx}\left(\frac{1}{\eta'(x)}f(x;\theta)\right).$$

It expresses a relative change of a basic component of the density, i.e., density divided by the Jacobian of mapping η. The t-score is a suitable function for using the generalized moment method for the estimation of parameters of heavy-tailed distributions. Let $X_1, \ldots, X_n$ be independent identically distributed (i.i.d) sample from F with probability density function (p.d.f.) f. The parametric version of the so-called t-mean, which can be considered as a measure of central tendency of distributions, yields the moment estimation equations for θ in the form

$$\frac{1}{n}\sum_{i=1}^{n} T(X_i;\theta) = 0.$$

The solution $\hat{\theta}$ is strongly consistent and asymptotically normal (see Fabián, 2001). For t-Hill estimator (Fabián and Stehlík, 2009), we have bounded score

$$S(x;\theta) = T_{\tilde{\eta}}(x;\theta) = \theta\left(1-\frac{\theta+1}{\theta x}\right)$$

and for generalized t-Hill estimator (Beran et al., 2014) (Pareto distribution and $\tilde{\eta}(x) = \ln(x-1), x>1$), we have the score

$$S(x;\theta,\beta) = \begin{cases} \theta\left(1-\frac{\theta+\beta-1}{\theta x^{\beta-1}}\right), & \text{for } \beta \neq 1, \\ \theta\left(\frac{1}{\theta}-\ln x\right), & \text{for } \beta = 1. \end{cases} \quad (1)$$

where $\beta > 0$ is tuning parameter. For $\beta = 2$ we obtain t-Hill, with "typical" transformation of the support of the distribution $(1, \infty)$ to the whole real line $(-\infty, \infty)$ is $\tilde{\eta}(x) = \ln(x-1), x>1$. Here an important inverse problem arises. For a given score $\tilde{S}$, does there exist one or several sufficiently smooth functions η such that equation

$$T_\eta = \tilde{S} \quad (2)$$

holds? Which qualitative properties do they posses?

Consider now the Pareto distribution with the probability density function (p.d.f.)

$$f(x,\theta) = \theta x^{-\theta-1}, \quad x>1$$

where $\theta > 0$ is a shape parameter (the tail index). Let us modify Eq. (2) by multiplying by $f > 0$ in order to receive exact 2nd-order differential equation in the form

$$h(x) + \frac{d}{dx}\left(\frac{f(x)}{\eta'(x)}\right) = 0, \quad (3)$$

where $h(x) = S(x;\theta, \beta) f(x)$. Now, integrate Eq. (3) to obtain an equation, which is solvable by quadrature, of the form

$$H(x) + \left(\frac{f(x)}{\eta'(x)}\right) = C,$$

where $H(x)$ is an antiderivative of h. Its form (under the condition $\beta \neq 1-\theta$) is:

$$H(x) = \theta^2 \int \left(1-\frac{\theta+\beta-1}{\theta x^{\beta-1}}\right)x^{-\theta-1}dx = \theta x^{-\theta}(x^{1-\beta}-1) + C_1.$$

This yields several classes[1] of solutions expressible in general in the form of special functions (a non-elementary antiderivatives). But this is an obstacle, since they can be hardly jointly analyzed because of their transcendental nature.

These difficulties motivate us to study Eq. (2), by a different approach, applicable for general density f and score function $\tilde{S}$. In order to analyze it is more convenient to define some extra variables $\mathbf{w} = (x,y,z) := (t+a, \eta, \eta'), a \in \mathrm{supp}(f) = \{x \in \mathbb{R}, : f(x) \neq 0\}$. Under the assumption $\eta' \neq 0$ Eq. (2) is equivalent to the system $\dot{\mathbf{w}} = \mathbf{W}(x,y,z)$, where $\mathbf{W}(x, y, z) = (1, z, \Psi(x, z))$, $\Psi(x,z) = z^2 S + z\frac{d}{dx}\ln(f(x))$ and $(x,y,z) \in D_0$, with $\mathcal{D}_0 := [a,\infty)\times[a,\infty)\times\mathbb{R}\setminus\{0\}$.

We use this approach in details for (3), where $a = 1$, $x \geq 1$ is the independent variable, $\eta(x) \geq 1$ is the unknown function with $\eta'(x) \neq 0$ and $(\beta, \theta) \in \mathbb{R}_+$ are parameters. In this way, (3) is equivalent to the following set of autonomous ordinary differential equations:

$$\begin{cases} \dot{x} = 1, \\ \dot{y} = z, \\ \dot{z} = \varphi(x,z), \end{cases} \quad (4)$$

where

$$\varphi(x,z) = -\frac{\theta+1}{x}z + \theta\left(1-\frac{\theta+\beta-1}{\theta x^{\beta-1}}\right)z^2,$$

and $(x,y,z) \in \mathcal{D}_0$.

In our setting any initial condition $(x_0, y_0, z_0) \in \mathcal{D}_0$ defines a unique smooth solution of (4)—and, hence, a unique differentiable solution $y = \eta(x)$ of (3). Each solution of (4) can be represented as a smooth orbit $\{(x(t), y(t), z(t))\}$ in $\mathbb{R}^3$ parameterized by $t \in \mathbb{R}$; see Guckenheimer and Holmes (1986) for more details.

The (unique) orbit through a given point $(x,y,z) \in \mathcal{D}_0$ is tangent to the vector $(1, z, \varphi(x, z))$ at the point (x, y, z). Hence, an orbit always flows forward in the direction of x and never "comes back" near any point already visited in the same orbit. More precisely, there is no dense orbit of (4) in any open region of the phase space $\mathbb{R}^3$. Hence, there cannot be topological mixing, which is one of the necessary ingredients of chaotic dynamics (Guckenheimer and Holmes, 1986; Hasselblatt and Katok, 2003).

For the fixed initial condition, we are able to obtain a monotonic solution for t-score for almost all possible cases of parameters. The t-score defines consistent estimator of tail parameter θ. The choice of parameter β is an issue of experience for the statistician/

[1] E.g. for $\beta = 1$ (Hill or MLE estimator) $\tilde{\eta}(x) = -\theta\ln\ln x + \text{const.}, x > 1$ is the example of η which can be expressed in terms of elementary functions.

ecologists. Experienced choice of parameter β brings a proper trade-off between robustness and efficiency (see Beran et al., 2014).

2.1. The qualitative behavior of the solutions

2.1.1. The function y = η(x) is monotone

The graph of $y = \eta(x)$ in the (x, y)-plane is determined by the initial condition (x_0, y_0, z_0) at $t = t_0$. In particular, from (4) it follows that z_0 is the initial slope $\eta'(x_0) = \dot{y}(t_0) = z_0$ of this solution. By the continuity of the solutions of (4), since $z = \eta'(x) \neq 0$, then

$$\operatorname{sign}(z_0) = \operatorname{sign}(z(t))$$

for all $t > 0$; namely, the sign of z_0 determines the (constant) sign of $\dot{y} = z$. Hence, $y(t)$ is a monotone function of t, and, hence, any solution $\eta(x)$ of (3) is either an increasing or decreasing function for every x. This is a very important property, since monotone transformations of data are statistically optimal.

2.1.2. The set $\varphi^{-1}(0)$

In spite of $\eta(x)$ being a monotone function, its graph could still have a number of different shapes, it could be bounded or unbounded, etc. Statistical reasons for having η a monotonic function are as follows: if we have a differentiable inverse of η we can compute the induced distribution after the transformation. From the ecological point of view, it is as parsimonious a view on ecological dynamics as one can consider.

In particular, the level set $\varphi^{-1}(0)$ in the (x, z)-plane determines the values of x where $\frac{d^2\eta(x)}{dx^2} = 0$ and, hence, where $\eta(x)$ has an inflection point. Moreover, the domain $\mathcal{D}_0$ of system (4) can be continuously extended in order to include the plane $z = 0$. Hence, in what follows we consider a continuous extension of the domain $\mathcal{D}_0$ given by

$$\mathcal{D}_1 := [1,\infty)\times[1,\infty)\times\mathbb{R}$$

so that the set

$$\mathcal{M}_0 := \{(x,z)\in[1,\infty)\times\mathbb{R} : z = 0\} \subset \varphi^{-1}(0).$$

In order to study $\varphi^{-1}(0)$, let us define the function

$$g(x) := \frac{\theta+1}{x(\theta-(\theta+\beta-1)x^{1-\beta})}, \tag{5}$$

and let $gr(g)$ be the graph of $z = g(x)$ in the domain $[1,\infty)\times\mathbb{R}$. Furthermore, let us define the following sets in the parameter space (β, θ):

$$\mathbf{\Omega}_1 = \{(\beta,\theta)\in\mathbb{R}_+ : 0<\beta<1, \theta+\beta-1<0\}; \tag{6}$$

$$\mathbf{\Omega}_2 = \{(\beta,\theta)\in\mathbb{R}_+ : 0<\beta<1, \theta+\beta-1>0\}; \tag{7}$$

$$\mathbf{\Omega}_3 = \{(\beta,\theta)\in\mathbb{R}_+ : 1<\beta<2\}; \tag{8}$$

$$\mathbf{\Omega}_4 = \{(\beta,\theta)\in\mathbb{R}_+ : 2<\beta\}; \tag{9}$$

and their boundaries:

$$\mathbf{T}_1 = \{(\beta,\theta)\in\mathbb{R}_+ : \theta+\beta-1 = 0\}; \tag{10}$$

$$\mathbf{T}_2 = \{(\beta,\theta)\in\mathbb{R}_+ : \beta = 1\}; \tag{11}$$

$$\mathbf{T}_2 = \{(\beta,\theta)\in\mathbb{R}_+ : \beta = 2\}. \tag{12}$$

The sets $\mathbf{\Omega}_k$, $k = 1, 2, 3, 4$ and $\mathbf{T}_j$, $j = 1, 2, 3$ are shown in panel (e) of Fig. 1. From a statistical point of view, by choosing of system (4) we decided for a specific form of dynamical system, driven by autonomous system for t-scores of Pareto distribution. Here we consider statistical learning based on t-score function with monotonous transformation η. From an ecological point of view, this was a convenient and parsimonious approach to model the underlying dynamics for extreme value estimators under the statistical constraints of Pareto tail, and a monotonous smooth η. The usefulness of Lemma 1 and Fig. 1 is that we can use the information on the nature of the set $\varphi^{-1}(0)$—as a function of parameters β and θ—to give some geometric insight into the possible shapes of $\eta(x)$ in terms of slope and inflection points. This will be greatly illustrated in the next subsection.

Fact: *The following statements hold, see Appendix C.1:*

Lemma 1.

1. *If $(\beta,\theta)\in\mathbf{\Omega}_1$, the set $\varphi^{-1}(0) = \{\mathcal{M}_0, \mathcal{M}_1\}$ consists of two branches, where $\mathcal{M}_1 = gr(g)$. The set $\varphi^{-1}(0)$ is qualitatively as in the sketch of Fig. 1(a).*
2. *If $(\beta,\theta)\in\mathbf{T}_1$, the set $\varphi^{-1}(0) = \{\mathcal{M}_0, \mathcal{M}_1\}$ consists of two branches, where $\mathcal{M}_1$ is the graph of $z = \frac{\theta+1}{\theta x}$. The set $\varphi^{-1}(0)$ is qualitatively as in the sketch of Fig. 1(b).*
3. *If $(\beta,\theta)\in\mathbf{\Omega}_2$, the set $\varphi^{-1}(0) = \{\mathcal{M}_0, \mathcal{M}_1, \mathcal{M}_2\}$ consists of three branches, where $\mathcal{M}_1\cup\mathcal{M}_2 = gr(g)$. The set $\varphi^{-1}(0)$ is qualitatively as in the sketch of Fig. 1(c).*
4. *If $(\beta,\theta)\in\mathbf{T}_2$, the set $\varphi^{-1}(0) = \{\mathcal{M}_0\}$ consists of the single branch $\mathcal{M}_0$. The set $\varphi^{-1}(0)$ is qualitatively as in the sketch of Fig. 1(d).*
5. *If $(\beta,\theta)\in\mathbf{\Omega}_3$, the set $\varphi^{-1}(0) = \{\mathcal{M}_0, \mathcal{M}_1, \mathcal{M}_2\}$ consists of three branches where $\mathcal{M}_1\cup\mathcal{M}_2 = gr(g)$. The set $\varphi^{-1}(0)$ is qualitatively as in the sketch of Fig. 1(f).*
6. *If $(\beta,\theta)\in\mathbf{T}_3$, the set $\varphi^{-1}(0) = \{\mathcal{M}_0, \mathcal{M}_1, \mathcal{M}_2\}$ consists of three branches where $\mathcal{M}_1\cup\mathcal{M}_2$ is the graph of $z = \frac{x(\theta+1)}{\theta x^2-(\theta+1)x}$. The set $\varphi^{-1}(0)$ is qualitatively as in the sketch of Fig. 1(g).*
7. *If $(\beta,\theta)\in\mathbf{\Omega}_4$, the set $\varphi^{-1}(0) = \{\mathcal{M}_0, \mathcal{M}_1, \mathcal{M}_2\}$ consists of three branches where $\mathcal{M}_1\cup\mathcal{M}_2 = gr(g)$. The set $\varphi^{-1}(0)$ is qualitatively as in the sketch of Fig. 1(h).*

2.1.3. The shapes of η(x)

In this section we describe the geometric properties of the function $y = \eta(x)$. We compute different solutions of (4) for fixed—and representative—values of (β, θ) in each parameter regime. The initial conditions are chosen of the form $(x_0, y_0, z_0) = (1, 1, z_0^{(k)})$, with $z_0^{(k)} \neq 0$. For each value of $z_0^{(k)}$, the graphs of $y = \eta_k(x)$ and $z = \eta_k'(x)$ correspond to the projection of the solution $(x_k(t), y_k(t), z_k(t))$ of (4) onto the (x, y) and (x, z)-planes, respectively.

Rather than computing each solution as mere integration from a given initial condition, we obtain each desired orbit $(x_k(t), y_k(t), z_k(t))$ with high accuracy as an element of a family of solutions of a well-posed boundary value problem—which is solved by continuation in Auto (Doedel et al., 2010); see also Doedel (2007). This numerical procedure is explained in Appendix C.5.

Figs. 2 and 3 show the graphs of a set of selected solutions $y = \eta_k(x)$ and $z = \eta_k'(x)$, where the index $k > 0$ if $z_0^{(k)} > 0$, and $k < 0$ if $z_0^{(k)} < 0$. Panels (a1) and (a2) of Fig. 2 show the projection of each solution to the (x, y) and (x, z)-plane, respectively, for $(\beta, \theta) = (0.5, 0.4) \in \mathbf{\Omega}_1$. Also shown in Fig. 2(a2) is the set $\varphi^{-1}(0) = \{\mathcal{M}_0, \mathcal{M}_1\}$ (gray lines); compare with Fig. 1(a). Similarly, Figs. 2(b1)–(b2), 3(a1)–(a2) and (b1)–(b2) show the corresponding graphs of $y = \eta_k(x)$ and $z = \eta_k'(x)$ (and the set $\varphi^{-1}(0)$) for $(\beta, \theta) = (0.5, 0.7) \in \mathbf{\Omega}_2$, $(\beta, \theta) = (1.5, 0.7) \in \mathbf{\Omega}_3$ and $(\beta, \theta) = (3, 0.7) \in \mathbf{\Omega}_4$, respectively.

Let us now describe in more details the properties of $y = \eta(x)$ in each scenario. In Fig. 2(a1), for $(\beta, \theta) \in \mathbf{\Omega}_1$, every solution $y = \eta_k(x)$ with positive initial slope $z_0^{(k)} > 0$ is a monotone increasing function. From Fig. 2(a2), the corresponding derivative functions $z = \eta_k'(x)$ grow unbounded at certain finite values $x_k^\infty < \infty$. Hence,

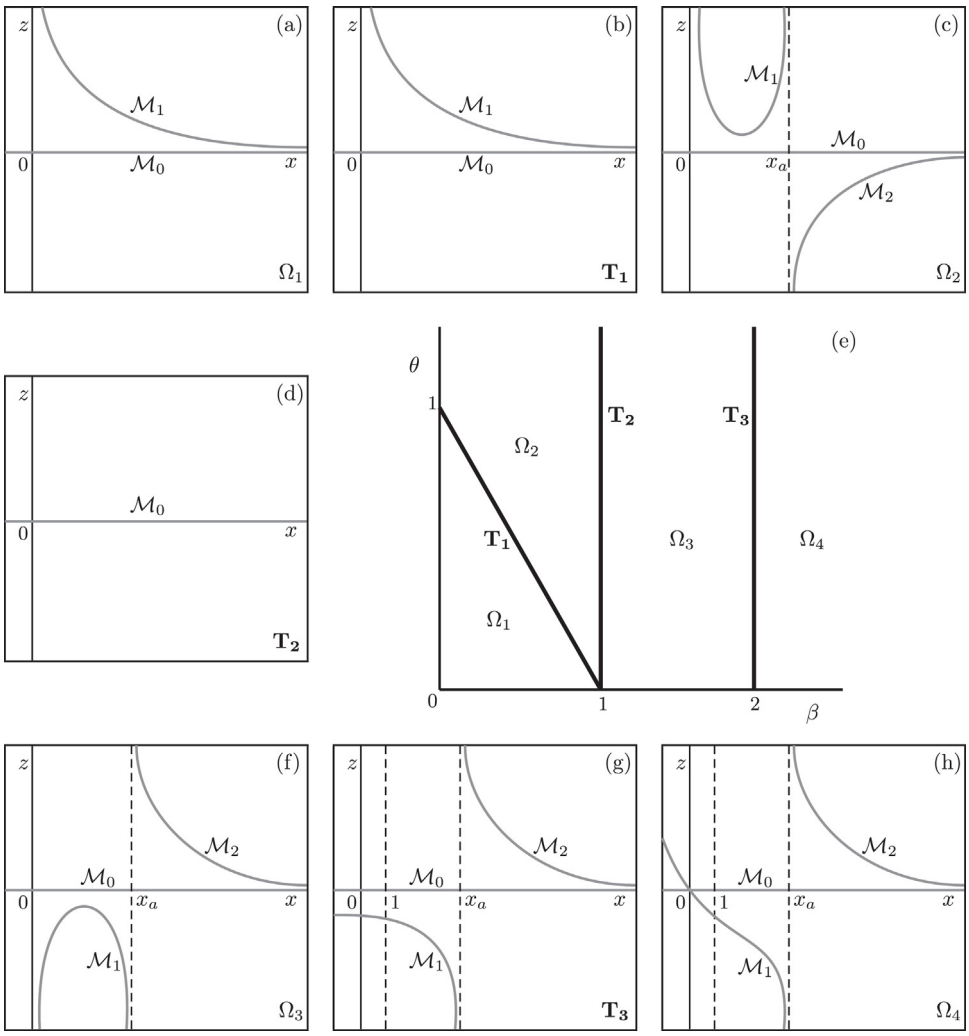

Fig. 1. Sketches of the set $\varphi^{-1}(0)$ in the (x, z)-plane (in panels (a)–(d) and (f)–(h)) for different parameter values (β, θ) in the regions shown in panel (e).

$\lim_{x \to x_k^\infty} \eta_k(x) = \infty$. On the other hand, in Fig. 2(a1) every solution $y = \eta_k(x)$ with negative initial slope $z_0^{(k)} < 0$ is a monotone decreasing function with bounded negative derivative—and, hence, $\eta_k(x)$ eventually changes sign and takes negative values—in fact, from Fig. 2(a2), the corresponding derivatives $z = \eta_k'(x)$ tend to $\mathcal{M}_0$ as $x \to \infty$.

In Fig. 2(b1), for $(\beta, \theta) \in \mathbf{\Omega}_2$, there exists a threshold initial slope $z_0^* > 0$ such that if $z_0^{(k)} > z_0^*$, the solution $y = \eta_k(x)$ grows unbounded much as in the previous case for $(\beta, \theta) \in \mathbf{\Omega}_1$; see the curve η_1 for instance. However, if $z_0^{(k)} < z_0^*$, the derivatives $z = \eta_k'(x)$ in panel (b2) start as increasing functions until they cross the curve $\mathcal{M}_1$ near certain point x_a (see Appendix C.1)—hence, attaining a maximum at the intersection point with $\mathcal{M}_1$—and decrease toward $\mathcal{M}_0$. As a consequence, the corresponding functions $y = \eta_k(x)$ have an inflection point and remain bounded; furthermore, each solution $y = \eta_k(x)$ tends to a horizontal asymptote $y = y_k^\infty$. On the other hand, the behavior of solutions for $z_0^{(k)} < 0$ for $(\beta, \theta) \in \mathbf{\Omega}_2$ is qualitatively as in $\mathbf{\Omega}_1$.

In Fig. 3(a2), for $(\beta, \theta) \in \mathbf{\Omega}_3$, if $z_0^{(k)} > 0$, the derivatives $z = \eta_k'(x)$ decay monotonously to $\mathcal{M}_0$ and fail to intersect the curve $\mathcal{M}_2$. On the other hand, if $z_0^{(k)} < 0$, the derivatives $z = \eta_k'(x)$ may not be monotonic functions—initially some of them are decreasing functions that cross the curve $\mathcal{M}_1$ to start to increase; see for instance η_{-1}', η_{-2}' and η_{-3}'—but eventually all of them tend monotonously toward $\mathcal{M}_0$. Therefore, in Fig. 3(a1), every curve $y = \eta_k(x)$ tends to a horizontal asymptote $y = y_k^\infty$; in particular, η_{-1}, η_{-2} and η_{-3} have an inflection point at certain value $x < x_{as}$ where $z = \eta_k'(x)$ crosses the curve $\mathcal{M}_1$. For $(\beta, \theta) \in \mathbf{\Omega}_4$, in Fig. 3(b1), virtually the same qualitative behavior of $y = \eta_k(x)$ is observed. In this last scenario, the only minor difference is that all the solutions $y = \eta_k(x)$ with negative initial slope $z_k^0 < 0$ have an inflection point as η_k' crosses the curve $\mathcal{M}_1$; see also Fig. 3(b2).

Finally, it remains to explore the shape of $y = \eta_k(x)$ when parameters (β, θ) cross from one open region to another in Fig. 1(e). However, notice that, if $(\beta, \theta) \in \mathbf{T_1}$, the set $\varphi^{-1}(0)$ is qualitatively as in the case for $(\beta, \theta) \in \mathbf{\Omega}_1$; one can expect $y = \eta(x)$ and $z = \eta'(x)$ to be qualitatively as in Fig. 2(a1) and (a2), respectively. Similarly, if $(\beta, \theta) \in \mathbf{T_3}$, the set $\varphi^{-1}(0)$ is qualitatively as in the case for $(\beta, \theta) \in \mathbf{\Omega}_4$ for $x \geq 1$; hence, the functions $y = \eta(x)$ and $z = \eta'(x)$ are qualitatively as in Fig. 3(b1) and (b2), respectively. Therefore, it only remains to see the case when $(\beta, \theta) \in \mathbf{T_2}$.

Fig. 4 shows the graphs of a set of solutions $y = \eta_k(x)$ and $z = \eta_k'(x)$ for $(\beta, \theta) = (2, 0.7) \in \mathbf{T_2}$. In panel (b), all the functions $z = \eta_k'(x)$ are monotonously decreasing (if $k > 0$) or increasing (if $k < 0$) toward $\mathcal{M}_0$ as $x \to \infty$. Thus, in panel (a), the functions $y = \eta_k(x)$ increase (if $k > 0$) or decrease (if $k < 0$) monotonously, and converge to a finite horizontal asymptote as $x \to \infty$. In Figs. 2–4 the evolutions of transformations $\eta(x)$ and their derivatives $z = \eta(x)$ are plotted. They, as a set form the statistical model "per se" in the sense of McCullagh (2002). Here we consider that to each transformation η a specific estimator and inference function (t-score) are given (see also Jordanova et al., 2016).

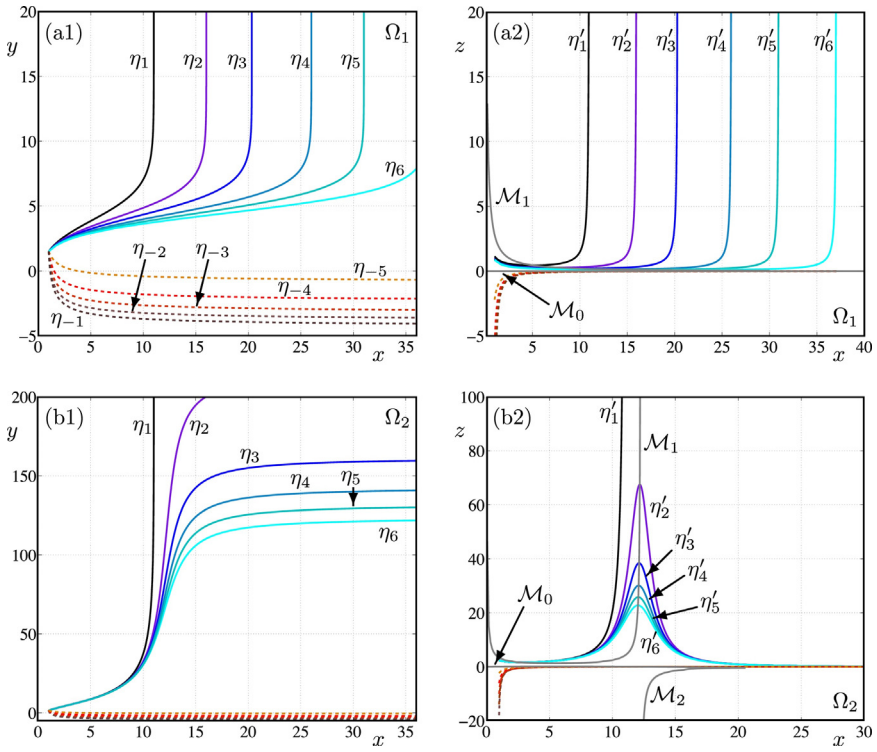

Fig. 2. The graph of the functions $y = \eta_k(x)$ and $z = \eta'_k(x)$—for different initial conditions—for $(\beta, \theta) = (0.5, 0.4) \in \Omega_1$ in panels (a1) and (a2), respectively, and for $(\beta, \theta) \in \Omega_2$ in panels (b1) and (b2), respectively.

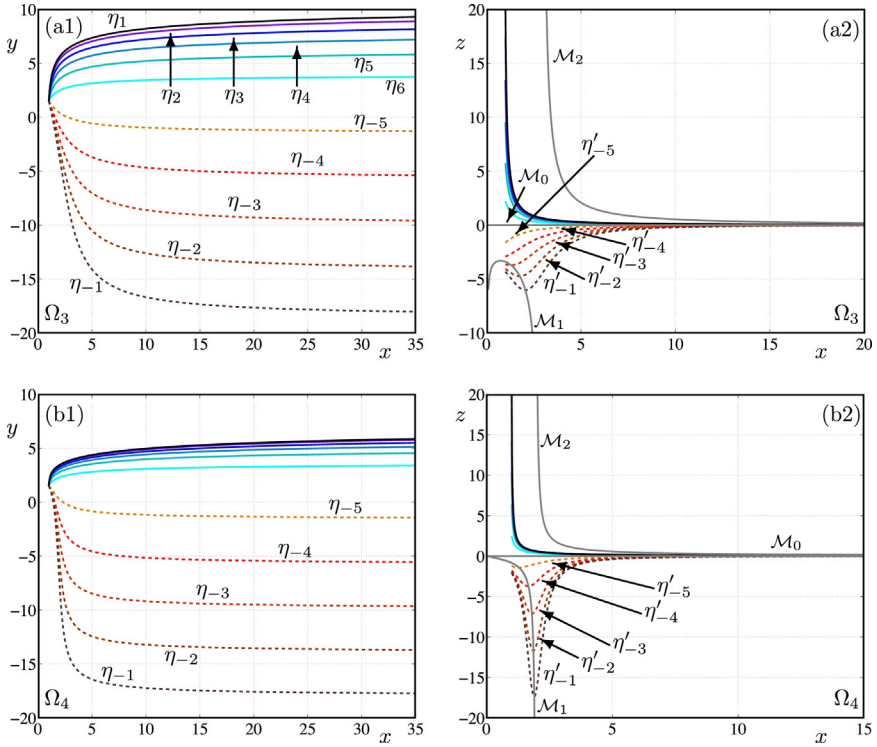

Fig. 3. The graph of the functions $y = \eta_k(x)$ and $z = \eta'_k(x)$—for different initial conditions—for $(\beta, \theta) = (1.5, 0.7) \in \Omega_3$ in panels (a1) and (a2), respectively, and for $(\beta, \theta) = (0.5, 0.7) = (3, 0.7) \in \Omega_4$ in panels (b1) and (b2), respectively.

3. Application 1: Guanaco Glacier

A glacier is a volume of snow and ice of area larger than 0.01 km^2, with evidences of flow, that is fed by solid water (snow, hail or hoarfrost), that is transformed into ice by densification and compaction, loosing mass mainly by melting, sublimation or calving. The balance between the gains and losses during a period of time (normally the hydrological year between April 1 and March 31 of the following year) is defined as Glacier Mass Balance (Kaser, 2003). For measuring this glacier mass balance, a number of stakes or poles are installed over a glacier (location determined mainly by the altimetry of the zone), where their protruding height is

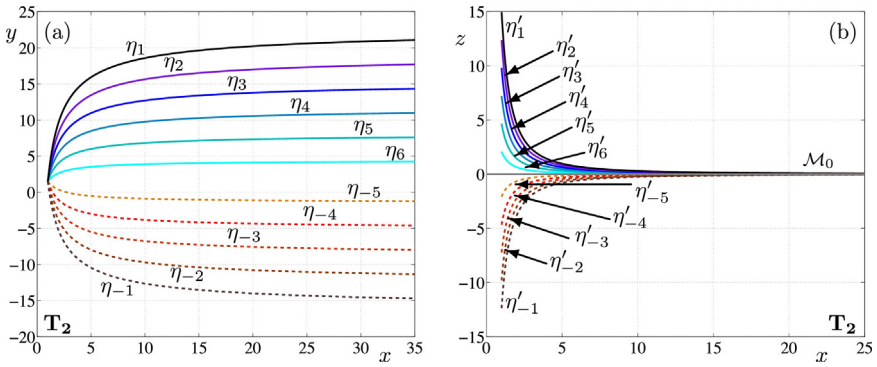

Fig. 4. The graph of the functions $y = \eta_k(x)$ and $z = \eta'_k(x)$—for different initial conditions—for $(\beta, \theta) = (2, 0.7) \in \mathbf{T_2}$ in panels (a) and (b), respectively.

repeatedly measured during each season together with the density of the intervening mass. The changes are converted into water equivalent by multiplying the pole heights by the density of the snow or ice gained or losses during the surveyed period. The mass balance per stake is then aggregated relative to the area of influence of each one, as in the following equation (Kaser, 2003)

$$B = \sum_i b_i \frac{s_i}{S}.$$

Guanaco glacier is located in the semi-arid region of Chile (latitude 29S) at an altitude range between 5000 and 5300 m above sea level, with a surface area of 1.61 km^2 in 2015 and a maximum thickness of 120 m (Rabatel et al., 2011). This glacier, together with other minor glaciers and glacierets (Fig. 5), is located close to Pascua Lama (Gascoin et al., 2011), a gold mining project that was interrupted in 2015. This mining project was monitoring these glaciers for environmental purposes since 2002 with the main aim of assessing possible impacts of their mining activities on the glacier mass balance among several other variables.

3.1. Estimators of the EVI

It is of interest to consider the statistical behavior of maxima $X_{n:n} = \max\{X_1, \ldots, X_n\}$, where the sequence of independent random variables $X_1, \ldots, X_n$ has the common cumulative distribution function F, that is $X_i \sim F$. The Fisher–Tippett–Gnedenko theorem (de Haan and Ferreira, 2006) shows us that if there exists a sequence of constants $\{a_n > 0\}$ and b_n such that

$$P\left(\frac{X_{n:n} - b_n}{a_n} \leq z\right) \to G(z) \text{ as } n \to \infty,$$

where $G(z)$ is a non-degenerate distribution function, then G corresponds to a Generalized Extreme Value distribution (GEV)

$$G(z) = \exp\left\{-\left[1 + \xi\left(\frac{z-\mu}{\sigma}\right)\right]^{-1/\xi}\right\}. \quad (13)$$

This result quite resembles the Central Limit Theorem, but now with the maximum of the sequence of random variables as the statistic of interest, not the average. The proof of this theorem can be found in Leadbetter et al. (1983), while a summary of some results with weaker hypothesis (such as loss of independency or stationarity) can be found in Coles (2001). This limiting cumulative distribution function (c.d.f.) $G(z)$ can be classified into three types according to its shape parameter ξ (called also EVI), these are often called Weibull ($\xi < 0$), Fréchet ($\xi > 0$) and Gumbell ($\xi = 0$) types. If, for example, F is such that G is a Weibull type, then it is said that F belongs to the Weibull Domain of Attraction of G, usually denoted as $F \in DA(G_\alpha)$. The shapes of these distributions for different parameters are given on Fig. 6. The practical relevant range of the EVI is $[-\frac{1}{2}, \frac{1}{2}]$.

In particular, several practical applications can be found in the case of the Weibull domain of attraction, for example, the ultimate world record in a specific athletic event given today's state of the art (Einmahl and Magnus, 2008), the estimation of the efficiency frontier in economics (Farrell, 1957) or the limit behavior of the distance of two random points over a convex set (Mayer and Molchanov, 2007). In general, the estimation of the finite right endpoint is linked to estimate $\xi < 0$.

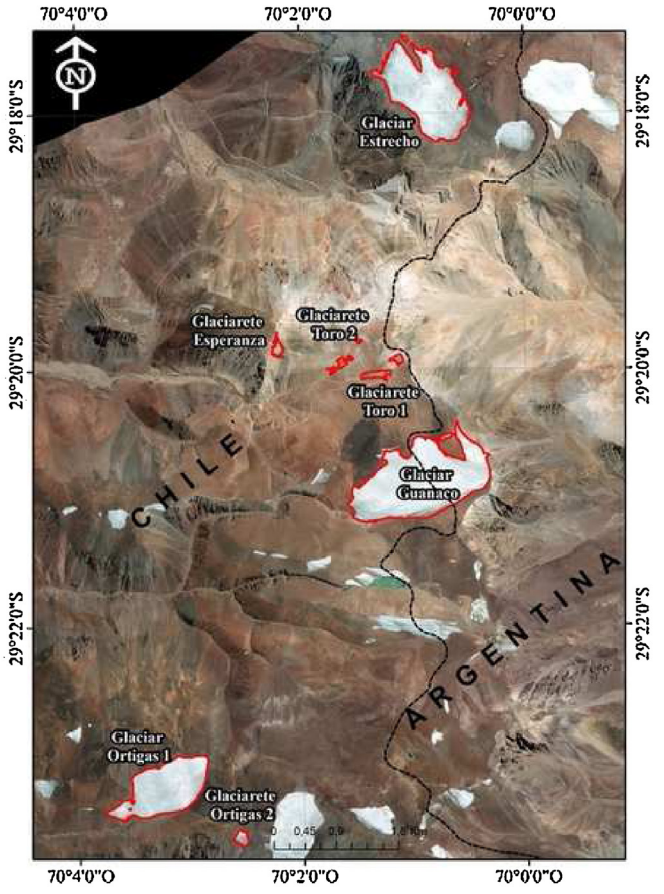

Fig. 5. Geographical location of glaciers nearby Guanaco glacier, the three largest are Guanaco, Estrecho and Ortigas 1; accounting for almost the 95% of the area of the 7 studied ice bodies.

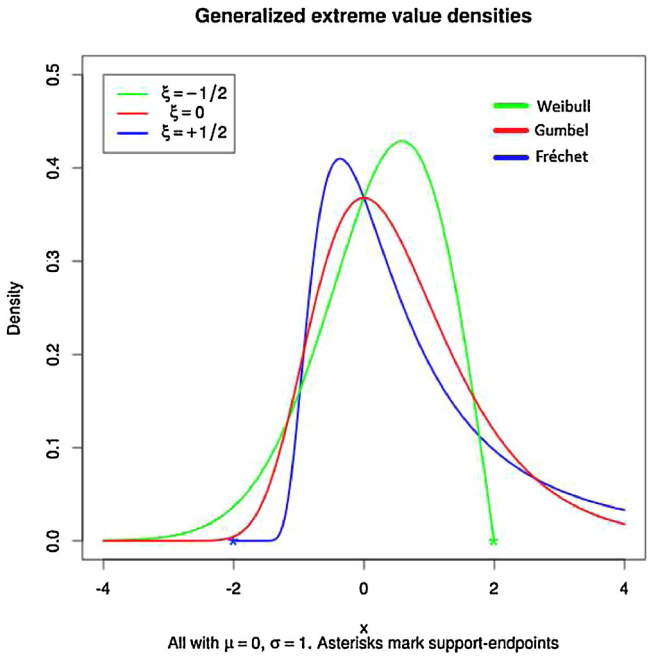

Fig. 6. Different behavior of the Generalized Extreme Value distribution according to the value of its shape parameter, the EVI.

If the previous theorem holds, then the conditional probability

$$P(X > u + y \mid X > u),$$

for large values of u, has a Generalized Pareto distribution (GP)

$$F(y) = 1 - \left(1 + \xi \frac{y}{\sigma}\right)^{-1/\xi}, \tag{14}$$

where $\sigma = \sigma + \xi(u - \mu)$, this limit c.d.f. can be also classified into three types, often called, Beta ($\xi < 0$), Pareto ($\xi > 0$) and Exponential ($\xi = 0$). This approach is known as Peaks over threshold (POT) (Coles, 2001) and suits better in a case when the whole data set is available and not only the maximum value of a predefined block. However, it is necessary to choose an appropriate threshold.

Several estimators were taken into account for this work. Here $X_{i:n}$ denotes the i-th order statistic of the sample $X_1, \ldots, X_n$, where $X_{n:n} = \max\{X_1, \ldots, X_n\}$ These estimators depend on the number of order statistics (k) which are used:

- An estimator based on the method of moments (Hosking and Wallis, 1987), labeled as **MOM**:

$$\hat{\xi}_{\text{MOM}}(k) = \frac{1}{2}\left(1 - \frac{\mu_0^2(k)}{\sigma^2(k)}\right),$$

where:

$$\mu_0(k) = \frac{1}{k}\sum_{i=1}^{k}[X_{n-i+1:n} - X_{n-k:n}],$$
$$\sigma^2(k) = \frac{1}{k-1}\sum_{i=1}^{k}[X_{n-i+1:n} - X_{n-k:n} - \mu_0(k)]^2.$$

- The method of probability weighted moments estimator (Hosking and Wallis, 1987), labeled as **PWM**, enjoys good properties in the small sample context (Furrer and Naveau, 2007):

$$\hat{\xi}_{\text{PWM}}(k) = 2 - \frac{\mu_0(k)}{\mu_0(k) - 2\mu_1(k)},$$

where $\mu_0(k)$ is defined as in the previous estimator, and:

$$\mu_1(k) = \frac{1}{k(k-1)}\sum_{i=1}^{k}(i-1)[X_{n-i+1:n} - X_{n-k:n}].$$

- Pickands' estimator (Pickands, 1975), labeled as **PICK**, is computed because it only needs four distinct order statistics (which makes it a robust estimator), and is location and scale invariant:

$$\hat{\xi}_{\text{PICK}}(k) = \frac{1}{\log 2}\log\left(\frac{X_{n-r_k+1:n} - X_{n-2r_k+1:n}}{X_{n-2r_k+1:n} - X_{n-4r_k+1:n}}\right),$$

where $r_k = \lfloor k/4 \rfloor$ with $\lfloor \cdot \rfloor$ the floor function.

- A moment estimator (Dekkers and de Haan, 1989), labeled as **m-Hill**:

$$\hat{\xi}_{\text{m-Hill}} = M_n^{(1)} + 1 - \frac{1}{2}\left(1 - \frac{(M_n^{(1)})^2}{M_n^{(2)}}\right)^{-1},$$
$$M_n^{(j)} = \frac{1}{k}\sum_{i=0}^{k-1}(\log X_{n-i:n} - \log X_{n-k:n})^j.$$

- Falk's estimator (Falk, 1995), labeled as **n-Hill**, defined as:

$$\hat{\xi}_{\text{n-Hill}} = \frac{1}{k}\sum_{i=1}^{k-1}[\log(X_{n:n} - X_{n-i:n}) - \log(X_{n:n} - X_{n-k:n})],$$
$$k \in \{1, \ldots, n-1\}.$$

3.2. Negative t-Hill estimator

The t-Hill estimator (Fabián and Stehlík, 2009) is a robust EVI estimator which works in the Fréchet domain of attraction, defined as:

$$\hat{\xi} = -1 + \left\{\frac{1}{k}\sum_{i=1}^{k}\frac{X_{k+1:n}}{X_{i:n}}\right\}^{-1}, \quad \text{where: } k \in \{1, \ldots, n-1\}.$$

This one is a particular case of the HME (Beran et al., 2014), which relates to the studied score function (1):

$$\hat{\xi} = H_{n:k}^{(\beta)} := \begin{cases} \frac{1}{\beta - 1}\left[\left(\frac{1}{k}\sum_{i=1}^{k}U_{ik}^{1-\beta}\right)^{-1} - 1\right], & \text{if } \beta > 1 \\ \frac{1}{k}\sum_{i=1}^{k}\log(U_{ik}), & \text{if } \beta = 1 \end{cases}$$

where $U_{ik} := \frac{X_{n-i+1:n}}{X_{n-k:n}}$.

In order to obtain a negative version of t-Hill estimator we applied a procedure similar to the one introduced by Falk (Falk, 1995; de Haan and Ferreira, 2006), resulting in the following estimator for the EVI, labeled as **n-t-Hill**:

$$\hat{\xi}_{\text{n-t-Hill}} = 1 - \left\{\frac{1}{k}\sum_{i=1}^{k}\frac{X_{n:n} - X_{n-i+1:n}}{X_{n:n} - X_{n-k:n}}\right\}^{-1}, \quad \text{where: } k \in \{2, \ldots, n-1\}.$$

In more detail, we have been considering the fact that if X belongs to the Weibull domain of attraction with $\xi < 0$, therefore, Y defined as:

$$Y = \frac{1}{x^* - X} \tag{15}$$

belongs to the Fréchet domain of attraction, i.e., $Y \in DA(G_{-\xi})$ (because $-\xi > 0$). In (15), x^* denotes the unknown value of the finite right endpoint, as an estimator of this value, the maximum observation of the sample was used, which is recommended for

$\xi < -\frac{1}{2}$ (de Haan and Ferreira, 2006). The following asymptotic results are detailed in Appendix A and proved in the Appendix:

$$\hat{\xi}_{\text{n-t-Hill}} \xrightarrow[k\to\infty]{P} \xi,$$

$$\sqrt{k}(\hat{\xi}_{\text{n-t-Hill}} - \xi) \xrightarrow[k\to\infty]{d} \mathcal{N}\left(0, \xi^2 \frac{(1-\xi)^2}{(1-2\xi)}\right), \qquad \xi < -\frac{1}{2},$$

$$k^{-\xi}(\hat{\xi}_{\text{n-t-Hill}} - \xi) \xrightarrow[k\to\infty]{d} \xi(1-\xi)\text{Weibull}\left(1, -\frac{1}{\xi}\right), \quad 0 > \xi > -\frac{1}{2}.$$

3.3. Computational Results

For this section, the chosen software was R (R Core Team, 2015), the code with the implementation of the estimation of a partially smooth c.d.f. was cordially shared by S. Müller and implemented in this work. All previous estimators were implemented plus their smoothed versions (Müller and Chhay, 2011), labeled with an "s" at the end of their names.

3.3.1. Small sample: Generalized Pareto distribution

In order to better contrast the results of Müller and Chhay (2011), the same setup was studied, that is, n random samples were generated from a Generalized Pareto (GP) distribution, with the parameters

$$\xi = \{-1, -0.75, -0.5, -0.25, -0.1\},$$

$\mu = 0$, $\sigma = 1$ with $n = \{16, 32, 64\}$ and a fixed seed for the random number generator (RNG) algorithm of value 200,905 the same that was used in Müller and Chhay (2011). The results are summarized in Table 1, which tries to resemble Müller and Chhay (2011, Table 3).

A similar behavior can be seen among different values of n, but there are more differences among them than in Müller and Chhay (2011), therefore, results for $n = \{16, 32, 64\}$ are shown and not only for $n = 32$. Smoothed estimators show great advantage over their non-smoothed counterparts, however, the lack of theoretical results about their order of convergence or their behavior over more general distributions, makes difficult to put smoothed estimators over non-smoothed ones in a more general view.

In the large sample case, the estimation is way more reliable than in the small one. One can observe here that all estimators are converging to the original value of the simulation, however, it can also be seen, the slower rate of convergence of both Negative t-Hill (n-t-Hill) and Falk's estimator (n-Hill) when $\xi < -0.5$, this result is expected given the asymptotic results obtained in this work.

3.4. Robustness testing for Pareto tails

The robust properties of t-Hill estimator have already been studied (Beran et al., 2014). They are explained by the fact that this estimator uses the harmonic mean instead of the Arithmetic one on the data. For this experiment, the c.d.f. of the contaminated samples is defined as:

$$F(x) = (1-\alpha)F_1(x) + \alpha F_2(x),$$

where F_1 is the c.d.f. of a transformed Pareto distribution (see Eq. (15)) of parameter $-\xi$ with $\xi < 0$, while F_2 is similar but with parameter $-\xi/2$.

Table 2 shows the relative efficiency of the estimators among themselves, for each value of $\alpha = \{0, 0.05, 0.1, 0.15, 0.2\}$ and $\xi = \{-0.1, -0.25, -0.5, -0.75\}$. The MSE and the percentage of contribution of each estimator to the global MSE is computed. The m-Hill estimator was left out due to its large MSE results. A starting value of $k = 10$ was chosen for the computation of the percentage, given the large instability of the estimation when almost all order statistics are taken into account.

It can be stated from the previous table that both n-Hill and n-t-Hill estimators are the only ones to perform better while the contamination level grows when $\xi > -0.75$. Also, it can be seen how all smoothed estimators are performing better than their non-smoothed counterpart when $\xi > -0.5$.

A similar analysis can be found in Table 3, but now taking the average of 20 order statistics around the optimal value of k for each estimator, the optimal was chosen given its MSE. A notion of relative stability can be obtained from these results if we make a comparison with Table 2, because a decrease in the percentage across the tables indicates a larger zone of reliable estimation of the EVI. This topic is quite important, because the optimal value of k is a topic of active research.

After a contamination both Negative t-Hill (n-t-Hill) and Falk's estimator (n-Hill) are almost invariant in their estimation, which clearly shows the robust properties of these estimators in this case of contamination. Estimation of the EVI on mass balance data of several glaciers from Pascua Lama region, from 2002 to 2014 can be found in Fig. 7. We can see from the values of several EVI estimators that for a complete modeling of the EVI on mass balance data from Pascualama region we need to consider several values of EVI, not only one.

4. Application 2: Extremal snow loads

Understanding of snow extremes plays an important role for both climatology and civil engineering. An approach combining engineering and climatology to assess accidental snow loads on structures is suggested in Sadovský et al. (2010). We use the data of collection and analysis of snow loads in Slovakia carried out recently (Sadovský et al., 2007, 2009). The long-term weekly measurements of snow water equivalent (SWE) of snow cover at rain-gauge stations are employed. Out of the rain-gauge stations,

Table 1
Best estimator according to MSE for different sample sizes and EVI. Estimators ending with "s" represent smoothed versions according to Müller and Chhay (2011).

ξ	$n = 16$		$n = 32$		$n = 64$	
	Best estimator(s)	Range(s) of k	Best estimator(s)	Range(s) of k	Best estimator(s)	Range(s) of k
−0.1	n-Hills MOMs	$k < 4$ $k \geq 4$	n-Hills MOMs	$k < 4$ $k \geq 4$	n-Hills MOMs	$k < 4$ $k \geq 4$
−0.25	n-Hills	All k	n-Hills	All k	n-Hills	All k
−0.5	n-Hills	All k	n-Hills n-t-Hills	$k < 8$ $k \geq 8$	n-Hills n-t-Hills	$k < 5$ $k \geq 5$
−0.75	n-t-Hills	All k	n-t-Hills	All k	n-t-Hills n-Hill	$k \leq 15$ $k > 15$
−1	n-t-Hills n-Hills	$k \leq 10$ $k > 10$	n-t-Hills n-Hill	$k < 7$ $k \geq 7$	n-t-Hills n-Hill	$k < 6$ $k \geq 6$

Table 2
Percentages of relative efficiency (the lesser the better) of each estimator for different levels of contamination and EVI. The minimum value can be seen in bold.

ξ	α	n-Hill	n-Hills	n-t-Hill	n-t-Hills	MOM	MOMs	PWM	PWMs	PICK	PICKs
−0.1	0	13.62	8.96	13.38	9.56	2.63	**1.56**	3.62	2.08	31.89	12.69
	0.05	13.55	8.96	13.33	9.53	2.68	**1.64**	3.68	2.19	31.58	12.87
	0.1	13.02	8.58	12.74	9.13	2.74	**1.72**	3.84	2.37	32.47	13.39
	0.15	12.53	8.38	12.32	8.90	2.82	**1.88**	4.05	2.64	32.58	13.91
	0.2	12.01	7.94	11.73	8.43	3.04	**2.11**	4.36	3.00	33.01	14.38
−0.25	0	9.50	2.48	9.71	3.30	4.34	**2.21**	5.91	3.14	43.01	16.39
	0.05	9.11	**2.33**	9.25	3.13	4.36	2.38	5.97	3.35	43.34	16.79
	0.1	8.56	**2.15**	8.68	2.91	4.57	2.65	6.23	3.70	43.32	17.23
	0.15	7.68	**1.92**	7.84	2.65	4.71	3.10	6.53	4.30	43.15	18.13
	0.2	6.85	**1.68**	6.98	2.37	5.04	3.66	7.01	5.02	42.56	18.85
−0.5	0	3.74	5.12	4.80	**2.94**	7.64	4.62	8.91	5.13	44.80	12.30
	0.05	3.27	5.37	4.26	**3.26**	7.38	4.88	8.78	5.45	44.56	12.78
	0.1	**2.84**	5.42	3.80	3.50	7.47	5.32	8.88	6.01	43.16	13.60
	0.15	**2.44**	5.30	3.38	3.64	7.58	5.91	9.11	6.72	41.34	14.59
	0.2	**2.12**	5.18	3.02	3.78	7.92	6.57	9.48	7.51	38.96	15.45
−0.75	0	**1.31**	22.60	2.18	16.12	6.47	8.30	6.50	7.59	23.11	5.81
	0.05	**1.19**	22.41	2.04	16.21	6.39	8.37	6.50	7.75	22.84	6.30
	0.1	**1.21**	21.75	2.04	15.99	6.47	8.51	6.65	8.01	22.40	6.98
	0.15	**1.25**	20.54	2.09	15.38	6.74	8.70	7.01	8.34	22.08	7.87
	0.2	**1.36**	19.17	2.23	14.64	7.17	8.94	7.46	8.73	21.47	8.84

Table 3
Percentages of relative efficiency (the lesser the better) of each estimator for different levels of contamination and EVI, taking into account 20 order statistics around the optimal MSE value. The minimum value can be seen in bold.

ξ	α	n-Hill	n-Hills	n-t-Hill	n-t-Hills	MOM	MOMs	PWM	PWMs	PICK	PICKs
−0.1	0	19.35	14.58	17.34	13.58	**1.22**	1.24	1.85	1.90	16.57	12.37
	0.05	18.41	13.84	16.31	12.74	**1.40**	1.55	2.23	2.21	17.40	13.91
	0.1	16.30	12.23	14.27	11.15	2.06	**2.02**	3.24	2.94	19.32	16.47
	0.15	14.15	10.67	12.29	9.63	2.53	**2.44**	4.10	3.62	21.91	18.68
	0.2	12.33	9.25	10.56	8.26	3.05	**2.91**	4.98	4.34	23.76	20.56
−0.25	0	13.95	4.71	11.51	4.35	**2.63**	2.70	3.95	4.04	30.41	21.76
	0.05	11.18	3.50	8.78	**3.05**	3.22	3.48	4.94	4.83	31.78	25.25
	0.1	8.11	2.33	6.02	**1.91**	4.43	4.45	6.70	6.05	32.83	27.17
	0.15	5.31	1.40	3.72	**1.08**	5.06	5.09	7.70	6.85	34.90	28.89
	0.2	3.43	0.83	2.22	**0.61**	5.50	5.49	8.33	7.47	36.31	29.80
−0.5	0	3.55	7.35	**2.73**	5.13	5.12	5.27	6.65	6.72	34.31	23.17
	0.05	1.63	8.67	**1.10**	6.89	5.74	5.95	7.44	7.21	31.45	23.92
	0.1	0.81	8.44	**0.74**	6.95	6.76	6.49	8.52	7.68	29.70	23.91
	0.15	**0.43**	4.67	0.46	44.40	4.10	4.07	5.38	4.79	17.79	13.91
	0.2	**0.49**	4.81	0.52	39.06	4.63	4.64	6.04	5.44	19.62	14.74
−0.75	0	**1.00**	31.47	1.14	19.10	4.52	4.43	5.05	4.77	17.83	10.68
	0.05	**0.84**	29.52	1.09	20.05	4.87	5.00	5.50	5.30	16.86	10.97
	0.1	**1.06**	26.15	1.32	19.38	6.00	5.42	6.84	5.68	17.74	10.41
	0.15	**1.13**	23.42	1.41	18.60	6.26	6.18	7.13	6.47	18.37	11.03
	0.2	**1.18**	21.69	1.44	18.14	6.45	6.69	7.39	6.94	18.99	11.09

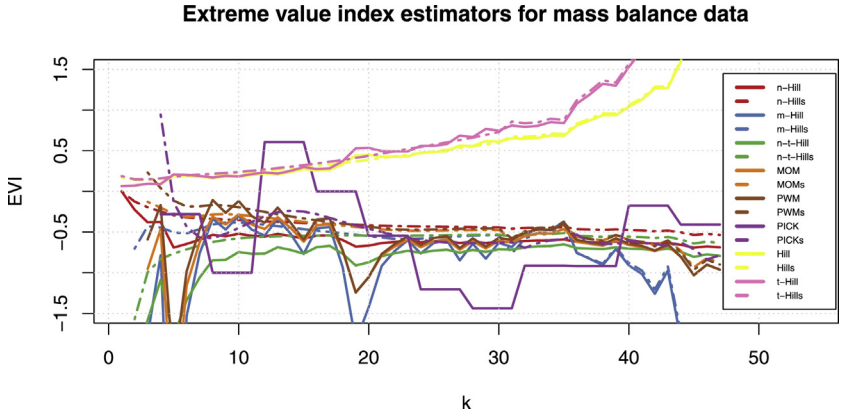

Fig. 7. EVI computed over the mass balance data of several glaciers from Pascualama region, from 2002 to 2014.

meteorological stations were selected at which daily SWE values have been recalculated using other climatological measurements, like depth of snow cover, etc. (see Sadovský et al., 2009). Preliminary statistical analysis has been made in Sadovský et al. (2010) and in Stehlík et al. (2015).

The SWE records of winter seasons are well suited for the assessment of the characteristic snow load on the ground, which is defined as 98% quantile of a suitable extreme value distribution fitted to the yearly snow load maxima. It is assumed that the maximum is a member of the same population, however, with a mean return period of say about 1000 years and more. Following Sanpaolesi et al. (1998) the largest snow load value is exceptional if the ratio k of the load to the characteristic snow load determined without that value is greater than 1.5. The snow loads identified as exceptional should be treated in accidental design situations as accidental actions (loads), cf. Eurocode EN 1990 (see Sanpaolesi et al., 1998).

The novelty of the approach for the assessment of the accidental snow loads by Sadovský et al. (2010) can be briefly described. First the k values in excess of 1.5 are identified. Then by the expertise of climatologists based on the geomorphology of Slovakia, regions of similar climate conditions for the occurrence of accidental snow loads are determined (see Fig. 8). Within a given region, the values of the empirical distribution function F restricted to the N ordered k values in excess of 1.5 is calculated as

$$F(k_i) = \frac{i}{N_R + 1}, \tag{16}$$

where N_R is the sum of winter seasons over all stations in the region and $i \in (N_R - N + 1, \ldots, N_R)$. The obtained empirical upper tail for k ratios is approximated, e.g. by nonlinear regression analysis using Pareto, exponential and Generalized Extreme Value (GEV) distributions. The extremes of 0.999 and 0.9999 quantiles of the distributions are of particular interest.

Under Generalized Pareto Distribution (GPD) with parameters μ, ξ and δ we get the distribution with c.d.f.

$$1 - \left(1 + \xi \frac{x-\mu}{\delta}\right)^{-1/\xi}, \quad x > \mu - \frac{\delta}{\xi}. \tag{17}$$

Under Generalized Extreme Value (GEV) distribution with parameters ξ, μ and δ we get the one with c.d.f.

$$\exp\left[-\left(1 + \xi \frac{x-\mu}{\delta}\right)^{-1/\xi}\right], \quad x > \mu - \frac{\delta}{\xi}. \tag{18}$$

We fit GPD to data from the companion paper (Sadovský et al., 2010). Particularly, we study regions of Slovakia separately. We refine the study of Regions 2 and the composite Region 4, within

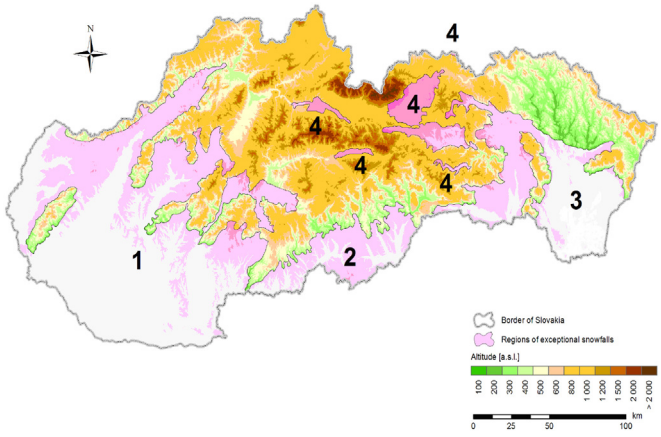

Fig. 8. Regions of exceptional snow loads (Sadovský et al., 2012).

Table 4
Maximum likelihood estimators of the parameters of GPD (17).

Parameter	Estimation	Standard error
ξ	0.3325008	0.2979518
δ	36.8023369	12.7791203

which the mountain basins are considered as one region. For the exceptional snow loads and their corresponding k values in Region 1, treated in Sadovský et al. (2012), a statistical dependence on the altitude is studied. The idea is to check the anticipated low dependence of k values on the altitude inferred from their definition, which comprises the altitude dependence already in the characteristic values.

4.1. Region 1

Here we consider 63 data, maximal values of the exceptional snow loads in Region 1, described in Stehlík et al. (2015), where a subset of these data is considered. We assume that the observations are independent. Their mean excess plot shows that the observed random variable has c.d.f. with Pareto tail. In order to fit the GPD to the exceedances of the threshold we use maximum likelihood approach, implemented in function *gpd.fit* in R. The threshold that we choose is $\mu = 97$. The number of exceedances is 28. The estimated values of the parameter ξ and δ of the c.d.f. (17) are given in Table 4. The GPD pp-plot of the exceedances is given on Fig. 9. It proves that we have made a good fit of the distribution of the data over the threshold.

In the above estimation we used only the upper order statistics of the observations in order to estimate the parameters. In this way we lose information about the observed values below the threshold 97. If we can estimate the c.d.f. in the entire range of the data it always would be better. Therefore, now we make a GEV fit of the data. The maximum likelihood approach is implemented in function *gev.fit* in R. The estimated values of the parameters μ, ξ and δ of the c.d.f. (18) are given in Table 5. Looking on the pp-plot on Fig. 10 we can conclude that this GEV (18) fit with the parameters, given in Table 5 is relatively good.

Both Hill on Fig. 11 and t-Hill plot on Fig. 12 confirmed the above values of the EVI, which is positive in this region.

4.1.1. Fitting the distribution of k in Region 1

Here we consider component k—the ratio of the load to the characteristic snow load determined without the largest snow load value for Region 1. The number of observations is again 63. The mean excess plot shows that the observed random variable has GPD with negative parameter ξ. In order to fit this distribution we use the maximum likelihood approach, implemented in function *gpd.fit* in R. For the threshold we use the minimal observed value

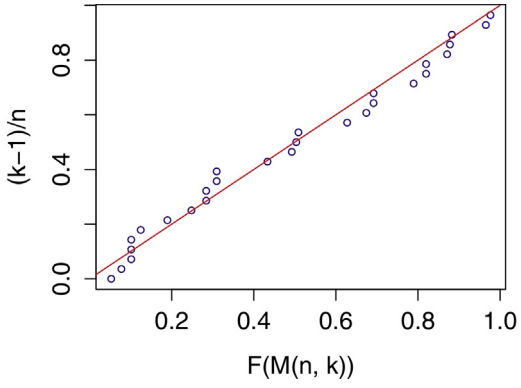

Fig. 9. GPD pp-plot of the maximal values of the exceptional snow loads in Region 1.

Table 5
Maximum likelihood estimators of the parameters of GEV (18).

Parameter	Estimation	Standard error
μ	85.5114413	3.34024537
ξ	0.3345636	0.09937401
δ	23.8166815	2.87468837

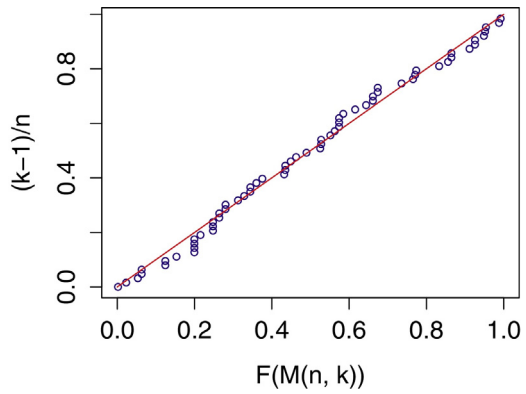

Fig. 10. GEV pp-plot of the maximal values of the exceptional snow loads in Region 1.

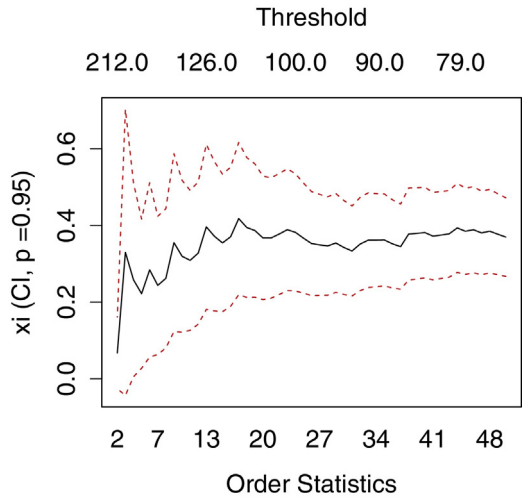

Fig. 11. Hill plot of the maximal values of the exceptional snow loads in Region 1.

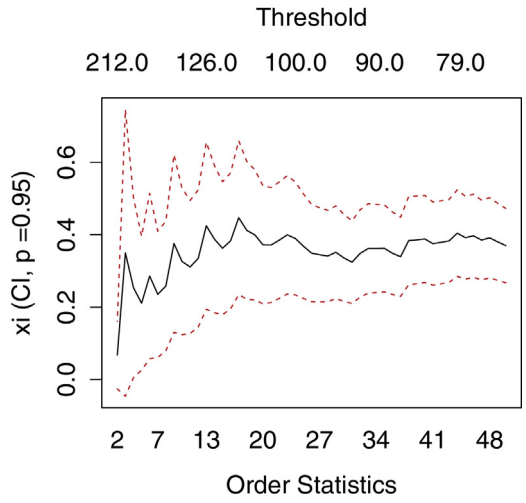

Fig. 12. t-Hill plot of the maximal values of the exceptional snow loads in Region 1.

Table 6
Maximum likelihood estimators of the parameters ξ and δ of the c.d.f. (18).

Parameter	Estimation	Standard error
ξ	−0.4606775	0.17744269
δ	0.2973319	0.06759829

μ = 1.5. The number of exceedances is 39. The estimated values of other parameters ξ and δ of the c.d.f. (18) are given in Table 6.

The pp-plot of the exceedances on Fig. 13 shows that our GPD fit of the distribution of the data is very good. The same conclusion could be made having in mind the similarity between the theoretical and empirical c.d.fs.

We can compare the Negative Hill estimator, proposed by Falk (1995) and the Negative t-Hill introduced in Section 3.3. Both, the Negative Hill like plot on Fig. 14 and the Negative t-Hill like plot on Fig. 15 confirmed the above values of the EVI.

4.2. Region 4

In contrast to the Region 1, where we have a relatively large amount of data, in Region 4 we have only 17 observations. Therefore, instead of using the functions *gev.git* and *gpd.fit* in R, we use the regression in order to estimate the coefficients in these distributions. This approach is considered in Stehlík et al. (2015) with respect to the distribution of k, where these data are

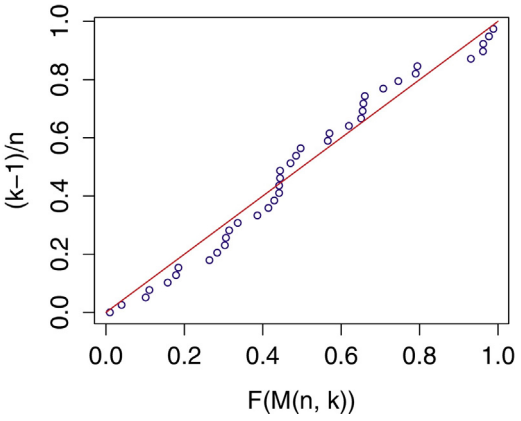

Fig. 13. GPD pp-plot of k in Region 1.

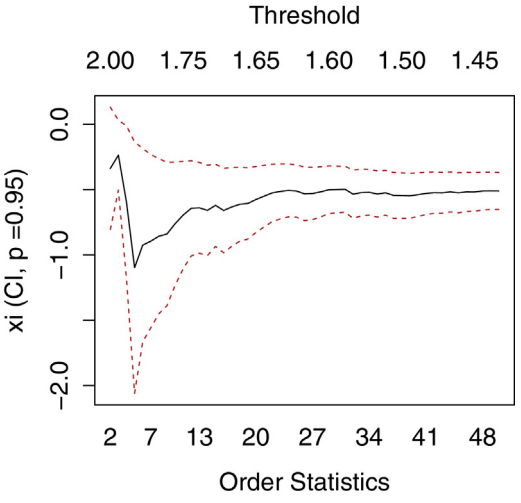

Fig. 14. Hill plot of k in Region 1.

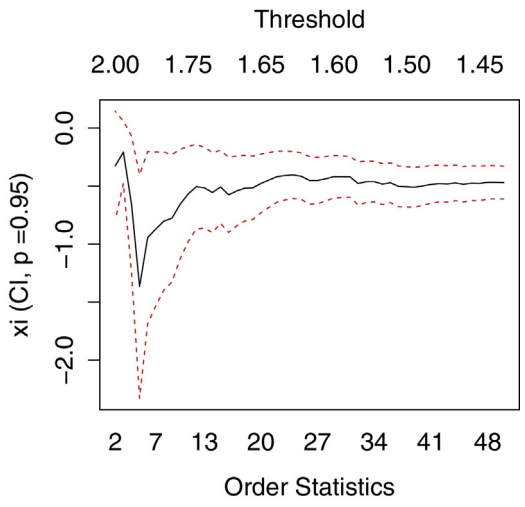

Fig. 15. t-Hill plot of k in Region 1.

considered. In order to simplify the regression model, instead of (17) we use the following definition for Pareto distribution

$$F(x) = 1-\left(\frac{\lambda}{x}\right)^{1/\xi}, \quad x>\lambda. \tag{19}$$

Under exponential c.d.f. we obtain

$$F(x) = 1-e^{-\frac{x-\mu}{a}}, \quad x>\mu. \tag{20}$$

The mean excess plot of the maximal values of the exceptional snow loads in Region 4 shows that the observed random variable has c.d.f. with Pareto tail. Here we compare three types of distributions for modeling these data: exponential type (20), Pareto type (19) and Generalized Extreme Value type (18). For the estimation of the coefficients we used *lm* function in R and the results are compared with the corresponding Hill and t-Hill estimators.

We start with the fitting of c.d.f. (19). Due to the fact that we have relatively small amount of data we will use for the threshold the minimal observed value. Having in mind that (20) is equivalent to

$$\log(1-F(x)) = \frac{\log\lambda}{\xi} - \frac{\log x}{\xi}, \quad x>\lambda$$

we make the following transformation of the data $F1 = \log(1 - cdf)$ and $X1 = \log sort(M)$, where cdf are the values in the empirical c.d.f. of the data and M denoted the Maximal snow load. The scatter plot of $F1$ and $X1$ is given on Fig. 16. Therefore, we use the regression model

$$F1 = \frac{\log\lambda}{\xi} - \xi^{-1}X1 + \varepsilon, \tag{21}$$

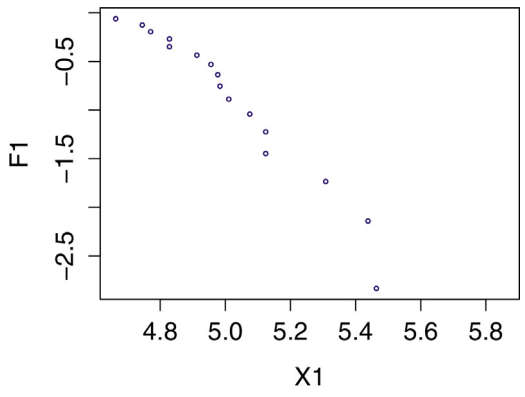

Fig. 16. Maximal values of the exceptional snow loads in Region 4.

Table 7
The estimators of the coefficients in (21).

Parameter	Estimation	Standard error	t value	Pr(>|t|)
$\log\lambda/\xi$	15.4089	1.0102	15.25	4.08e−10
$-1/\xi$	−3.2565	0.2013	−16.18	1.87e−10

Table 8
Estimators of the coefficients in GEV of the error term in (21).

Parameter	Estimation	Standard error
μ	0.01233436	1.999988e−06
ξ	0.19224841	2.150387e−03
δ	−1.02813582	1.999988e−06

where ε is the random error. The estimators of the coefficients are given in Table 7. Both are statistically significant. Residual standard error of the model is 0.1841 on 14 degrees of freedom. We have the multiple $R^2 = 0.9492$ and adjusted $R^2 = 0.9456$. The empirical value of the Fisher characteristic is 261.7. Its p-value is 1.866e−10. The degrees of freedom are correspondingly 1 and 14. The latter means that this model is adequate. The normal qq-plot of the error terms on Fig. 17 shows that the distribution of the error term in the last regression is not a normal one. The GEV qq-plot on Fig. 18 shows that the observed random variable is GEV distributed. The estimators of the coefficients in (18) are given in Table 8. Now we come back to the initial coefficients and obtain that $\xi = 0.3070782$ and $\lambda = 113.4926$. The qq-plot on Fig. 19 shows the quality of this fit. The confidence intervals are wide then we also apply GPD and GEV models.

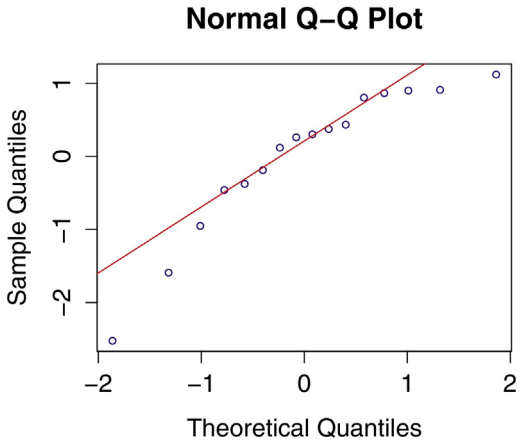

Fig. 17. Normal qq-plot of the error terms in model (21).

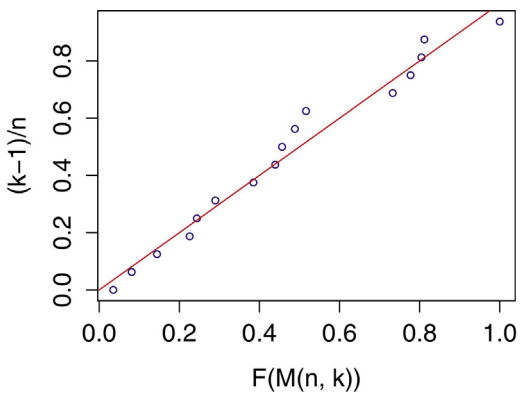

Fig. 18. GEV qq-plot of the error terms in model (21).

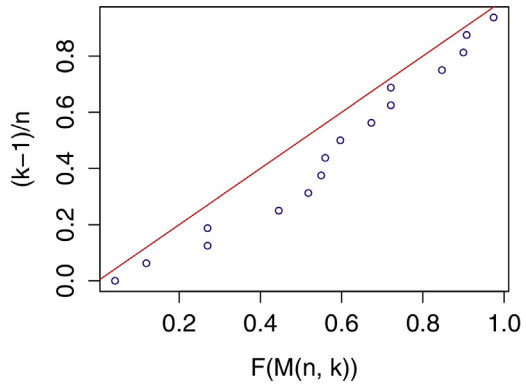

Fig. 19. Exponential (see (19)) qq-plot of the maximal snow loads in Region 4.

We can use Hill and t-Hill estimators in order to obtain the estimated value of ξ. Depending on the number of upper order statistics that are included in the estimators, the Hill and t-Hill plots are given correspondingly in Figs. 20 and 21.

Now we will use the fact that the Pareto distribution appears mainly in exceedances over high threshold. We use the function *gpd.fit* in R, over the threshold 140 and obtain that the parameter μ in (17) is equal to 140, and the estimators of ξ and δ are given in Table 9. The qq-plot on Fig. 22 shows that this fit could be useful.

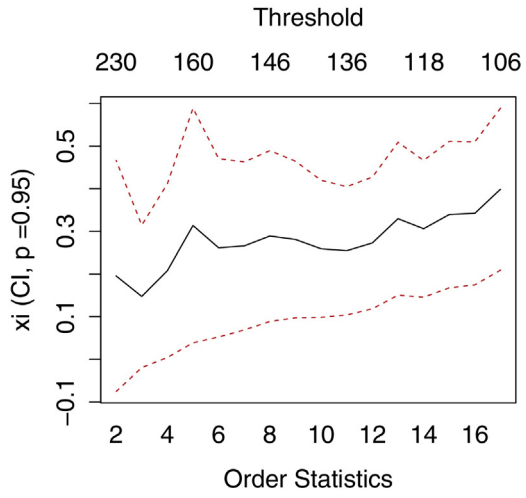

Fig. 20. Hill plot of the maximal values of the exceptional snow loads in Region 4.

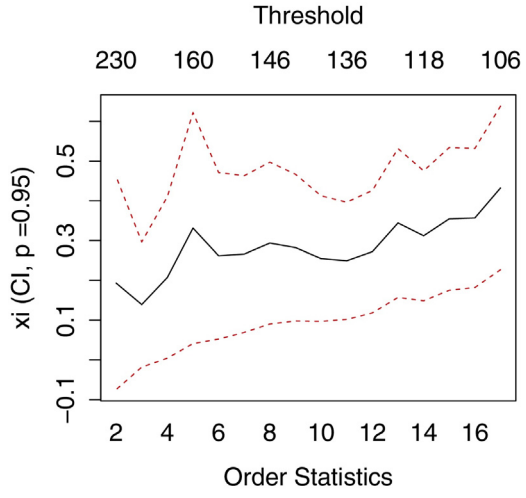

Fig. 21. t-Hill plot of the maximal values of the exceptional snow loads in Region 4.

Table 9
Estimators of the coefficients in GPD of the error term in (17).

Parameter	Estimation	Standard error
ξ	0.3319058	0.5106394
δ	35.3014497	20.6332138

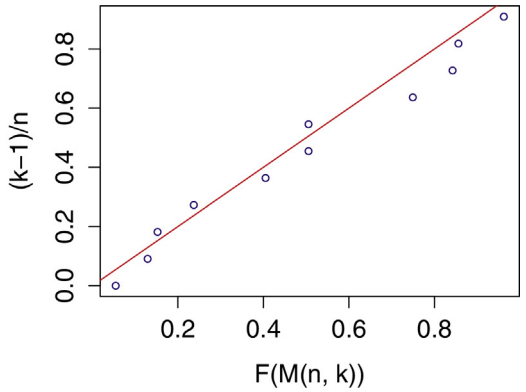

Fig. 22. GPD pp-plot of the maximal values of the exceptional snow loads in Region 4, threshold 140.

Table 10
Estimators of the coefficients in GPD of the error term in (17).

Parameter	Estimation	Standard error
ξ	−0.02649701	0.2509478
δ	61.52754876	21.4716669

Now we use the same approach including all the values. Although the sample size is only 17, we use the function *gpd.fit* in R, over the threshold 105.99 and we obtain $\mu =$ 105.99 in (17); $\hat{\xi}$ and δ are given in Table 10. In this case we have very wide confidence intervals. The qq-plot is given on Fig. 23.

The differences in Pareto predictions show again the well known fact that if we use a small amount of data and the distribution of the observed variable is not exact Pareto, the Pareto fit is not stable. Therefore we make GEV (18) fit of the data. The estimated values of the parameters μ, ξ and δ of the c.d.f. are given in Table 11. ξ still has wide confidence intervals, however μ and δ are statistically significant. The pp-plot on Fig. 24 shows that this fit is relatively good.

We make also exponential fit with c.d.f. (20). The minimal observed value is 106. According to Balakrishnan and Basu (1996)

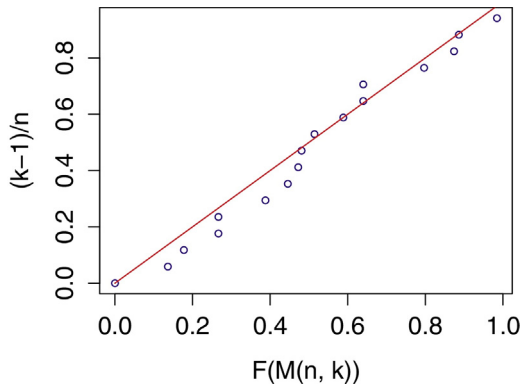

Fig. 23. GPD pp-plot of the maximal values of the exceptional snow loads in Region 4, threshold 105.99.

Table 11
The estimators of the parameters in the GEV (18) model.

Parameter	Estimation	Standard error
μ	136.1595290	8.0254567
ξ	0.3673421	7.0589241
δ	28.3571790	0.2482327

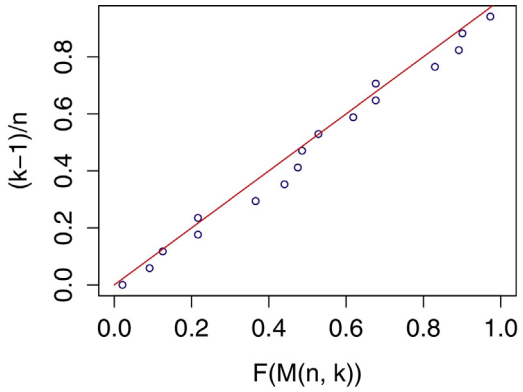

Fig. 24. GEV pp-plot of the maximal values of the exceptional snow loads in Region 4.

this is the estimator for μ. Again by Balakrishnan and Basu (1996), the best estimator for scale a is

$$\widehat{a} = \frac{17(X_n - 106)}{16} = \frac{17(165.9 - 106)}{16} = 63.64375.$$

The corresponding exponential pp-plot, given on Fig. 25 shows that again we observe a good fit.

4.3. Region 2

In Region 2 we have only 9 observations. Here we proceed with fitting the distributions of the maximal snow loads and k in this region.

The maximal values of the exceptional snow loads in Region 2 are given on Fig. 26. In sense of reproducible research we present the data

```
m 144 86 88 110 84 101 80 89 97
```

Although we have very small amount of data their mean excess plot on Fig. 27, shows that the observed random variable is possibly to have a c.d.f. with Pareto tail. In order to fit the Generalized Pareto Distribution (GPD) to the exceedances of the threshold we use maximum likelihood approach, implemented in

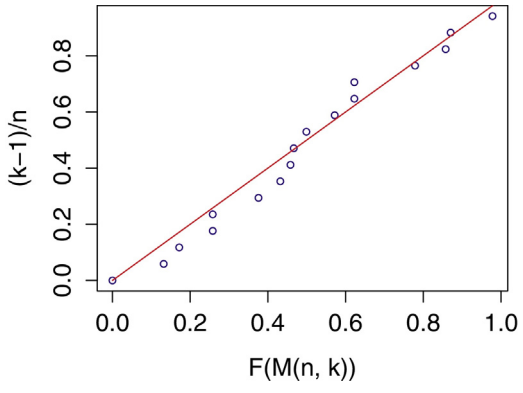

Fig. 25. Exponential pp-plot of the maximal values of the exceptional snow loads in Region 4.

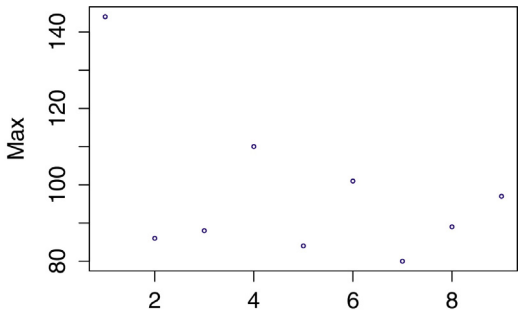

Fig. 26. Maximal values of the exceptional snow loads in Region 2.

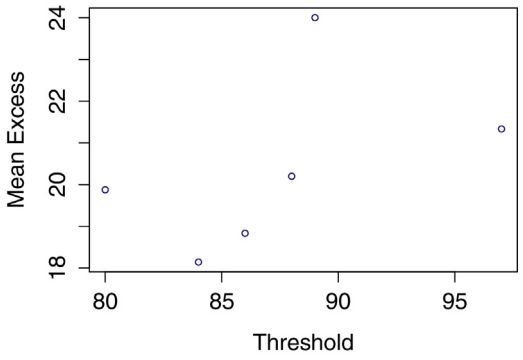

Fig. 27. Mean excess plot of the maximal values of the exceptional snow loads in Region 2.

function *gpd.fit* in R. The threshold that we choose is the minimal observation that is 85. The number of exceedances is 7. The estimated value of the parameter ξ and δ of the c.d.f.

$$1 - \left(1 + \xi \frac{x - 85}{\delta}\right)^{-1/\xi}, \quad x > 85 - \frac{\delta}{\xi} \tag{22}$$

are given in Table 12. Due to the small number of observations we have wide confidence intervals. The pp-plot of the exceedances is given on Fig. 28 the corresponding c.d.f. are in Fig. 29. It proves that we have made a relatively good fit of the distribution of the data over the threshold.

Table 12
The estimated value of the parameter ξ and δ of the c.d.f. (22).

Parameter	Estimation	Standard error
ξ	0.1905593	0.583140
δ	14.0443152	9.705665

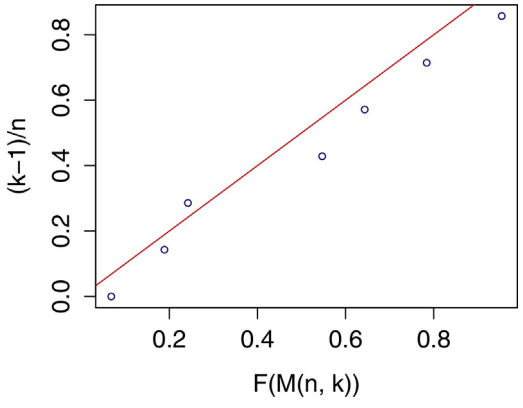

Fig. 28. GPD pp-plot of the maximal values of the exceptional snow loads in Region 2.

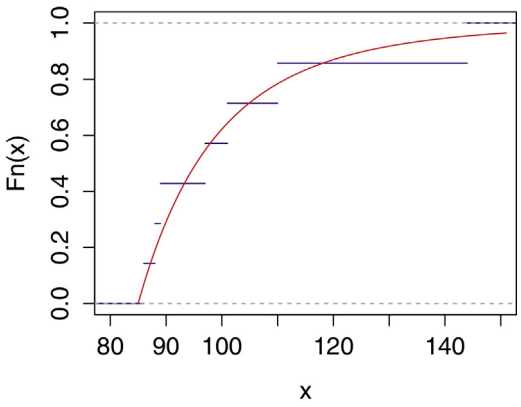

Fig. 29. Empirical c.d.f. and the corresponding estimated GPD c.d.f.

Table 13
The estimated values of the parameters μ, ξ and δ of the c.d.f. (18).

Parameter	Estimation	Standard error
μ	87.6472012	3.2619087
ξ	0.4756571	0.3795467
δ	8.2649512	3.0653720

As we have already mentioned, if we can estimate the c.d.f. in all range of the data it always would be better. Therefore now we make a GEV fit of the data. More precisely we estimate the parameters of the c.d.f. (18). We use the function *gev.fit* in R and obtain the estimated values of the parameters μ, ξ and δ of the c.d.f. (18). They are given in Table 13. Looking on Fig. 31 we can compare the theoretical GEV c.d.f (18) with the parameters, given in Table 13, with the empirical c.d.f. of the observed data. This together with the pp-plot on Fig. 30 shows that this fit is better than the GPD fit.

4.3.1. Fitting the distribution of k *in Region 2*

Here we consider component k - the ratio of the load to the characteristic snow load determined without the largest snow load value for Region 2. In sense of reproducible research we present the data

```
k 1.72 1.60 1.46 1.42 1.32 1.29 1.24 1.22 1.17
```

The mean excess plot of the data shows that the observed random variable has GEV distribution therefore we estimate the parameters of the c.d.f. (18). The estimated values of the parameters μ, ξ and δ of the c.d.f. (18) are given in Table 14. Looking on Fig. 33 we can compare the theoretical GEV c.d.f (18) with the parameters, given in Table 14, with the empirical c.d.f. of the observed data. This together with the pp-plot

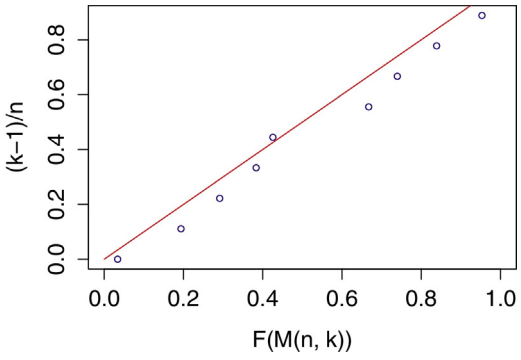

Fig. 30. GEV pp-plot of the maximal values of the exceptional snow loads in Region 2.

Table 14
The estimated values of the parameters μ, ξ and δ of the c.d.f. (18).

Parameter	Estimation	Standard error
μ	1.2868780	0.04976148
ξ	0.2239521	0.44424346
δ	0.1177385	0.04137990

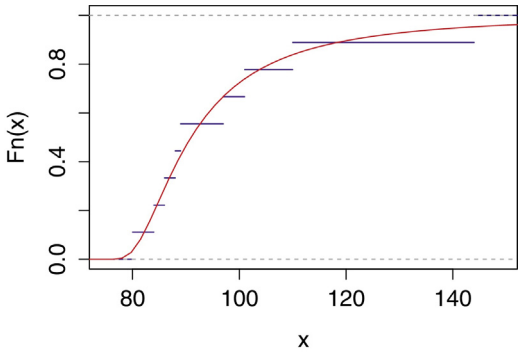

Fig. 31. Empirical c.d.f. and the corresponding estimated GEV c.d.f.

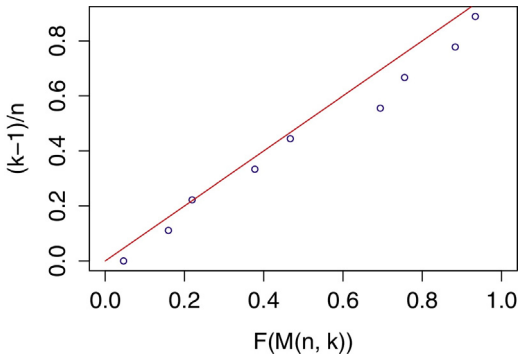

Fig. 32. GPD pp-plot of the values of k in Region 2.

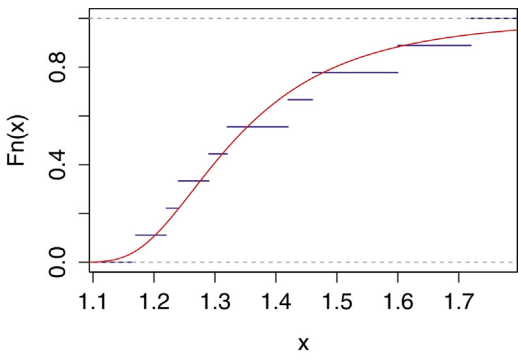

Fig. 33. Empirical c.d.f. and the corresponding estimated GEV c.d.f.

on Fig. 32 shows that although the confidence intervals of the coefficients are wide this fit is good.

5. Conclusions

It is clear that oscillations of natural ecological systems are measured imprecisely. To this imprecision contribute both non-chaotical and chaotical dynamical systems. In the present paper we explained non-chaotical dynamics of autonomous system of t-scores, which underline statistical estimates of entropy. Other source of contribution is switching between negative and positive extreme value indexes. This is well visible from both applications, Guanaco glacier in Chile and extreme snow loads in Slovakia. These observations provide new illustrations of the decomposition in

deterministic, stochastic and chaotic parts introduced in Stehlík et al. (2016). Therein we studied the methane emission example and we outlined the problem of deceptiveness regarding a complete certainty of the climate change. Several other contributions to imprecision can be made by fusion of several p-values (Baker, 2016).

More care should be taken in interpretations and the use of various observations of the climate change as well as in their methodologies and approaches.

Thus based on these new observations, we doubt the possibilities of a 100% judgment (a 100% paradigm of expectations) that the climate change has been caused solely by human effect. The currently obtained consensus of 95–98% to justify a human impact on the global climate change is probably the maximal possible threshold.

Acknowledgements

Milan Stehlík acknowledges the support of Fondecyt Proyecto Regular No. 1151441. Pablo Aguirre was partially funded by Fondecyt grant 11150306 and Proyecto Basal CMM Universidad de Chile. Andrés Rivera was supported by CECs which is funded by the Chilean government through the Centers of Excellence Base Financing Program of Comisión Nacional de Investigación y Tecnología de Chile (CONICYT). This work was also supported by the Slovak Research and Development Agency under the contract No. SK-AT-2015-0019. Jozef Kisel'ák was partially supported by grant VEGA MŠ SR 1/0344/14.

Appendix A. General information

Let $X, X_1, \ldots, X_n$ be independent random variables with common c.d.f. F. In the following, we assume that:

(A.1) F belongs to the maximum domain of attraction of the Weibull distribution.

This assumption entails that F has a finite right endpoint x^* and that F has a negative EVI $\xi < 0$. Our goal is to estimate ξ. To this end, the so-called n-t-Hill estimator is considered:

$$\hat{\xi} = 1 - \left(\frac{1}{k} \sum_{i=0}^{k-1} \frac{X_{n:n} - X_{n-i:n}}{X_{n:n} - X_{n-k:n}} \right)^{-1},$$

where $X_{1,n} \le \cdots \le X_{n,n}$ are the ordered statistics associated with $X_1, \ldots, X_n$ and $k \in \{1, \ldots, n\}$.

Introducing the auxiliary random variable $Z := (x^* - X)^{-1}$ and denoting by G its c.d.f., extreme-value theory shows that G belongs to the maximum domain of attraction of the Fréchet distribution. Under **(A.1)**, G has an infinite right endpoint and a positive EVI given by $-\xi$. Additionally, the tail quantile function of Z defined by

$$U(\cdot) := (1-G)^{\leftarrow}(1/\cdot) = 1/(x^* - (1-F)^{-1}(1/\cdot))$$

is regularly varying with index $-\xi$, i.e.

$$U(tx)/U(t) \to x^{-\xi} \text{ as } t \to \infty \text{ for all } x > 0. \tag{A.1}$$

See Bingham et al. (1987) for a general account on regular variation. In extreme-value theory, the second order condition aims at quantifying the rate of convergence in **(A.1)**:

(A.2) There exist $\rho < 0$ and some positive or negative function A with $A(t) \to 0$ as $t \to \infty$ such that

$$\frac{1}{A(t)} \left(\frac{x^{\xi} U(tx)}{U(t)} - 1 \right) \to \frac{x^{\rho} - 1}{\rho} \text{ as } t \to \infty \text{ all } x > 0.$$

See for instance (de Haan and Ferreira, 2006, p. 74).

Appendix B. Main properties

Our main result establishes an asymptotic representation for the n-t-Hill estimator in terms of Weibull and Gaussian random variables. To this end, recall that the Weibull distribution with parameter $\theta > 0$ denoted by $W(\theta)$ is defined by the c.d.f.

$$F_\theta(x) = 1 - \exp(-x^\theta), \quad x > 0.$$

Theorem 1. *Suppose* **(A.2)** *holds and let* $\theta = \min(1/2, -\xi)$. *Let* $k \to \infty$ *such as* $k/n \to 0$ *and* $k^\theta A(n/k) \to \lambda \in \mathbb{R}$ *as* $n \to \infty$. *Then, the following asymptotic expansion holds*

$$k^\theta(\hat{\xi} - \xi) = k^{\theta - 1/2} \frac{\xi(1-\xi)}{\sqrt{1}} \zeta (1 + o_P(1)) + k^{\theta+\xi} (1-\xi)\xi \zeta_\xi (1 + o_P(1)) + \frac{\lambda(1-\xi)}{1-\rho-\xi}(1 + o_P(1)),$$

where ζ *is a standard Gaussian random variable and* ζ_ξ *is a random variable following the Weibull distribution* $W(-\xi)$.

As a consequence, two different cases appear:

Corollary 1. *Assume that the assumptions of Theorem 1 hold with* $\lambda = 0$.

(i) *If* $\xi < -1/2$, *then* $k^{1/2}(\hat{\xi} - \xi)$ *is asymptotically Gaussian centered with variance* $\xi^2(1-\xi)^2/(1-2\xi)$.
(ii) *If* $\xi > -1/2$, *then* $k^{-\xi}(\hat{\xi} - \xi)$ *converges in distribution to* $(1-\xi)^2 W(-1/\xi)$.

As a comparison, let us stress that the asymptotic distribution of the n-Hill estimator defined by

$$\xi_{\leftarrow} = \frac{1}{k} \sum_{i=1}^{k-1} \log(X_{n:n} - X_{n-i+1:n}) - \log(X_{n:n} - X_{n-k:n})$$

(see for instance de Haan and Ferreira, 2006, paragraph 3.6.2) has been established only for $\xi \in (-1, -1/2)$ whereas Theorem 1 holds for all $\xi < 0$. Under the assumptions of Theorem 1 and assuming $\xi \in (-1, -1/2)$, it has been shown that

$$k^{1/2}(\xi_{\leftarrow} - \xi) = \xi \zeta (1 + o_P(1)) + \frac{\lambda\xi}{\rho(1-\rho)(1+\xi)}(1 + o_P(1)),$$

where ζ is a standard Gaussian random variable, see de Haan and Ferreira (2006, Theorem 3.6.4). It is thus possible to compare the asymptotic behavior of $\hat{\xi}$ and $\xi_{\leftarrow}$ for $\xi \in (-1, -1/2)$. First, it is clear that $\hat{\xi}$ has a larger asymptotic variance (given by $\xi^2(1-\xi)^2/(1-2\xi)$) than $\xi_{\leftarrow}$ (which is ξ^2). It is possible to show that $\hat{\xi}$ has a smaller asymptotic bias (given by $(1-\xi)/(1-\rho-\xi)$) than $\xi_{\leftarrow}$ (which is $\xi/(\rho(1-\rho)(1+\xi))$) for all $\xi \le \xi_0$ where $\xi_0 = \frac{1-\rho-\sqrt{(1-\rho)(1-5\rho+4\rho^2-4\rho^3)}}{2(\rho^2-\rho-1)}$. In particular, the asymptotic bias of $\xi_{\leftarrow}$ explodes when ξ approaches -1 while the asymptotic bias of $\hat{\xi}$ remains bounded.

Finally, note that, in case (ii) even when $\lambda = 0$, $\hat{\xi}$ has a negative asymptotic bias given by $(1-\xi)\xi\Gamma(1-\xi)k^{\xi}$. Nevertheless, this bias can easily be estimated and corrected.

Appendix C. Proofs

C.1. Reasoning of Lemma 1

From the Implicit Function Theorem, for every $z_0 \neq 0, x_0 \ge 1$, the equation $\varphi(x, z) = 0$ implicitly defines the function $z = g(x)$ near

(x_0, z_0), provided $\theta-(\theta+\beta-1)x_0^{1-\beta}\neq 0$. Hence, the graph of $g(x)$ determines branches of the set $\varphi^{-1}(0)$.

If $(\beta,\ \theta)\in\Omega_1$, let $u=x^{1-\beta}$. Then, the graph of $q(u):=\theta-(\theta+\beta-1)u$ is a straight line with positive slope $-(\theta+\beta-1)$. Since $q(0)=\theta>0$, then $q(u)>0$ for every $u\geq 0$. It follows that $\theta-(\theta+\beta-1)x^{1-\beta}>0$ and, hence, $g(x)>0$ and its graph on the positive (x, z)-plane consists of a single branch $\mathcal{M}_1$. Moreover, one can readily check that $\lim_{x\to 0^+}g(x)=\infty$ and $\lim_{x\to\infty}g(x)=0$. In addition,

$$g'(x)=-\frac{(\theta+1)F(x)}{x^2(\theta-(\theta+\beta-1)x^{1-\beta})^2}, \tag{C.1}$$

where

$$F(x)=\theta+(\beta-2)(\theta+\beta-1)x^{\beta-1}. \tag{C.2}$$

Since $F(x)>0$ for every $(\beta,\theta)\in\Omega_1$, then $g(x)$ is a strictly monotone decreasing function. In this way, the set $\varphi^{-1}(0)$ consists of the two branches $\mathcal{M}_0$ and $\mathcal{M}_1$, where $\mathcal{M}_1$ is defined as the graph of $g(x)$, that is, $\mathcal{M}_1=\{(x,z): z=g(x)\}$. A qualitative sketch of the set $\varphi^{-1}(0)$ is shown in Fig. 1(a).

If $(\beta,\theta)\in\mathbf{T}_1$, we have $\varphi(x, z)=z\,T_1(x, z)$, with

$$T_1(x,z)=\left(-\frac{\theta+1}{x}+\theta z\right).$$

Hence, (adopting the same notation of Ω_1) the set $T_1^{-1}(0)=\{\mathcal{M}_1\}$ where $\mathcal{M}_1$ is the hyperbola given by $z=(\theta+1)/(\theta x)$; see the qualitative sketch in Fig. 1(b).

If $(\beta,\theta)\in\Omega_2$, from (5) it follows that the line

$$x_{as}=\left(\frac{\theta+\beta-1}{\theta}\right)^{\frac{1}{\beta-1}}$$

is a vertical asymptote of $\varphi^{-1}(0)$. Hence, the graph of $z=g(x)$ consists of two branches. Let $\mathcal{M}_1$ and $\mathcal{M}_2$ be the branches defined for $x<x_{as}$ and $x>x_{as}$, respectively. Then, it is easy to see that $g(x)>0$ for $x<x_{as}$, and $g(x)<0$ for $x>x_{as}$. Moreover, $\lim_{x\to 0^+}g(x)=\infty$ and $\lim_{x\to\infty}g(x)=0$. Furthermore, from (C.1) and (C.2) it follows that $g(x)$ has a local minimum at $x_{\min}=\frac{(2-\beta)(\theta+\beta-1)}{\theta}=(2-\beta)^{\frac{1}{\beta-1}}x_{as}<x_{as}$. On the other hand, $g'(x)>0$ for every $x>x_{as}$; hence, $\mathcal{M}_2$ is defined by a strictly increasing function. As a consequence, the graph of $\varphi^{-1}(0)$ if $(\beta,\theta)\in\Omega_2$ is qualitatively as in Fig. 1(c).

The analysis for the other cases is similar.

C.2. Auxiliary lemmas

The following lemma provides an expansion of the t-Hill estimator in terms of two random variables $T_{1,n}$ and $T_{2,n}$ which derive its asymptotic distribution.

Lemma 2. *Under* **(A.1)**, *the n-t-Hill estimator can be rewritten as*

$$\frac{1}{1-\hat{\xi}}-\frac{1}{1-\xi}=\frac{T_{1,n}-\frac{1}{1-\xi}}{1-T_{2,n}}+\frac{\xi}{1-\xi}\frac{T_{2,n}}{1-T_{2,n}},$$

with

$$T_{2,n}=\frac{U(Y_{n-k:n})}{U(Y_{n:n})},$$
$$T_{1,n}=\frac{1}{k}\sum_{j=0}^{k-1}\frac{U(Y_{n-k:n})}{U(Y_{n-j:n})},$$

and where $Y_{1:n}\leq\cdots\leq Y_{n:n}$ are ordered statistics associated with n independent standard Pareto random variables.

The next lemma provides some consequences of the second order condition **(A.2)**.

Lemma 3. *Under* **(A.2)**, *there exists a function A_0 asymptotically equivalent to A such that, for all $\varepsilon>0$ there exists $t_0>0$ such that, for all $t\geq t_0$ and $x\geq 1$,*

$$\frac{x^\xi U(tx)}{U(t)}=1+R_1(t,x)A_0(t), \tag{C.3}$$

$$\frac{U(t)}{U(tx)}=x^\xi-\frac{x^{\xi+\rho}-x^\xi}{\rho}A_0(t)-x^\xi R_0(t,x)A_0(t)+R_2(t,x)A_0^2(t), \tag{C.4}$$

with

$$\begin{aligned}|R_0(t,x)| &\leq \varepsilon x^{\rho+\varepsilon},\\ |R_1(t,x)| &\leq \varepsilon-1/\rho,\\ |R_2(t,x)| &\leq 4(\varepsilon^2+1/\rho^2)x^\xi.\end{aligned}$$

We first establish the asymptotic distribution of $T_{1,n}$.

Lemma 4. *Let $k\to\infty$ such that $k/n\to 0$ as $n\to\infty$. Then, under* **(A.2)**, *$k^{-\xi}T_{1,n}\xrightarrow{d}\zeta_\xi$ where ζ_ξ is a random variable following the Weibull distribution $W(-1/\xi)$.*

Second, we focus on the asymptotic distribution of $T_{2,n}$.

Lemma 5. *Let $k\to\infty$ such that $k/n\to 0$ as $n\to\infty$. Then, under* **(A.2)**,

$$T_{2,n}\overset{d}{=}\frac{1}{1-\xi}+\sigma(\xi)k^{-1/2}\zeta(1+o_P(1))+\tau(\xi,\rho)A(n/k)(1+o_P(1)),$$

where ζ is a standard Gaussian random variable, $\tau(\xi,\rho)=\frac{1}{(1-\xi)(1-\rho-\xi)}$ and $\sigma(\xi)=\frac{\xi}{(1-\xi)\sqrt{1-2\xi}}$.

C.3. Proofs of auxiliary lemmas

Proof of Lemma 2. Introducing $Z_j=(x^*-X_j)^{-1}$ for $j=1,\ldots,n$, the n-t-Hill estimator can be rewritten as

$$\frac{1}{1-\hat{\xi}}\overset{d}{=}\frac{1}{k}\sum_{j=0}^{k-1}\frac{X_{n:n}-X_{n-j:n}}{X_{n:n}-X_{n-k:n}}=\frac{\frac{1}{k}\sum_{j=0}^{k-1}\frac{Z_{n-k:n}}{Z_{n-j:n}}-\frac{Z_{n-k:n}}{Z_{n:n}}}{1-\frac{Z_{n-k:n}}{Z_{n:n}}}.$$

Besides, $\{Z_j\}_{j=1,\ldots,n}\overset{d}{=}\{U(Y_j)\}_{j=1,\ldots,n}$ where $Y_1,\ldots,Y_n$ is a sample of independent random variables from a standard Pareto distribution. Therefore,

$$\frac{1}{1-\hat{\xi}}\overset{d}{=}\frac{T_{2,n}-T_{1,n}}{1-T_{1,n}}$$

and the conclusion follows.

Proof of Lemma 3. From de Haan and Ferreira (2006, Theorem B.2.18), it is possible to control the rest in the convergence **(A.2)**: There exists a function A_0 asymptotically equivalent to A such that, for all $\varepsilon>0$ there exists $t_0>0$ such that, for all $t\geq t_0$ and $x\geq 1$,

$$|R_0(t,x)|:=\left|\frac{1}{A_0(t)}\left(\frac{x^\xi U(tx)}{U(t)}-1\right)-\frac{x^\rho-1}{\rho}\right|\leq\varepsilon x^{\rho+\varepsilon}.$$

Letting $R_1(t, x):=(x^\rho-1)/\rho+R_0(t, x)$, it follows that

$$\frac{x^\xi U(tx)}{U(t)}=1+R_1(t,x)A_0(t),$$

with $|R_1(t,x)|\leq\varepsilon-1/\rho$ for all $t\geq t_0, x\geq 1$ and $\varepsilon<-\rho$. The first part (C.3) of the lemma is proved.

It straightforwardly follows that

$$\frac{U(t)}{U(tx)} = x^{\xi} - x^{\xi}R_1(t,x)A_0(t) + \frac{x^{\xi}R_1^2(t,x)A_0^2(t)}{1+R_1(t,x)A_0(t)}$$
$$= x^{\xi} - x^{\xi}\frac{x^{\rho}-1}{\rho}A_0(t) - x^{\xi}R_0(t,x)A_0(t) + \frac{x^{\xi}R_1^2(t,x)A_0^2(t)}{1+R_1(t,x)A_0(t)}.$$

Finally, letting $R_2(t,x) := x^{\xi}R_1^2(t,x)/(1+R_1(t,x)A_0(t))$, one has

$$|R_2(t,x)| \le 2(\varepsilon^2 + 1/\rho^2)x^{\xi}/(1-(\varepsilon - 1/\rho)|A_0(t)|).$$

Since, for t large enough, $|A_0(t)| \le 1/(2\varepsilon - 2/\rho)$, the second part (C.4) of the lemma follows.

Proof of Lemma 4. Applying expansion (C.3) of Lemma 3 with $t = Y_{n-k:n} \xrightarrow{P} \infty$ (see de Haan and Ferreira, 2006, Corollary 2.2.2) and $x = Y_{n:n}/Y_{n-k:n} \ge 1$ yields

$$\left(\frac{Y_{n:n}}{Y_{n-k:n}}\right)^{\xi}\frac{U(Y_{n:n})}{U(Y_{n-k:n})} = 1 + O_P(A_0(Y_{n-k:n})) = 1 + O_P(A(Y_{n-k:n}))$$
$$= 1 + o_P(1),$$

in view of de Haan and Ferreira (2006, page 75). As a consequence of Rényi representation, $Y_{n:n}/Y_{n-k:n} \stackrel{d}{=} Y^*_{k:k}$ where $Y^*_{k:k}$ is the maximum of a k-sample from a standard Pareto distribution. We thus have $T_{1,n} \stackrel{d}{=} (Y^*_{k:k})^{\xi}(1 + o_P(1))$. Moreover, the extreme-value theorem states that $Y^*_{k:k}/k$ converges in distribution to the extreme-value distribution Φ_1 (see for instance Embrechts et al., 1987, Table 3.4.2) with c.d.f. $\psi_1(x) = \exp(-1/x)$, $x > 0$. It is therefore easily seen that $k^{-\xi}T_{1,n} \xrightarrow{d} \Phi_1^{\xi} = W(-1/\xi)$.

Proof of Lemma 5. Applying expansion (C.4) of Lemma 3 with $t = Y_{n-k:n} \xrightarrow{P} \infty$ (see de Haan and Ferreira, 2006, Corollary 2.2.2) and $x = Y_{n-j:n}/Y_{n-k:n} \ge 1$, $j = 0, \ldots, k-1$ yields the expansion

$$T_{2,n} = T_{3,n} - T_{4,n} - T_{5,n} + T_{6,n} \tag{C.5}$$

with

$$T_{3,n} = \frac{1}{k}\sum_{j=0}^{k-1}\left(\frac{Y_{n-j:n}}{Y_{n-k:n}}\right)^{\xi},$$
$$T_{4,n} = \frac{A_0(Y_{n-k:n})}{\rho}\ \frac{1}{k}\sum_{j=0}^{k-1}\left(\left(\frac{Y_{n-j:n}}{Y_{n-k:n}}\right)^{\xi+\rho} - \left(\frac{Y_{n-j:n}}{Y_{n-k:n}}\right)^{\xi}\right),$$
$$T_{5,n} = A_0(Y_{n-k:n})\ \frac{1}{k}\sum_{j=0}^{k-1}\left(\frac{Y_{n-j:n}}{Y_{n-k:n}}\right)^{\xi} R_0\left(Y_{n-k:n}, \frac{Y_{n-j:n}}{Y_{n-k:n}}\right),$$
$$T_{6,n} = A_0^2(Y_{n-k:n})\ \frac{1}{k}\sum_{j=0}^{k-1} R_2\left(Y_{n-k:n}, \frac{Y_{n-j:n}}{Y_{n-k:n}}\right).$$

The four terms are studied separately. In view of Rényi representation, $(Y_{n-j:n}/Y_{n-k:n})_{j=0,\ldots,k-1} \stackrel{d}{=} (Y^*_{k-j:k})_{j=0,\ldots,k-1}$ where $Y^*_1, \ldots, Y^*_k$ is a sample of independent random variables from the standard Pareto distribution and $Y^*_{1:k} \le \cdots \le Y^*_{k:k}$ are the associated ordered statistics. Consequently, $T_{3,n}$ can be rewritten as

$$T_{3,n} \stackrel{d}{=} \frac{1}{k}\sum_{j=0}^{k-1}(Y^*_{k-j:k})^{\xi} = \frac{1}{k}\sum_{j=1}^{k}(Y^*_j)^{\xi},$$

Remarking that $\mathbb{E}((Y^*_1)^{\xi}) = 1/(1-\xi)$ and $\mathrm{var}((Y^*_1)^{\xi}) = \sigma^2(\xi)$, the central limit theorem entails that

$$T_{3,n} = \frac{1}{1-\xi} + k^{-1/2}\sigma(\xi)\zeta(1 + o_P(1)), \tag{C.6}$$

where ζ is a standard Gaussian random variable. Let us now focus on $T_{4,n}$. First, remark that

$$A_0(Y_{n-k:n}) = A(Y_{n-k:n})(1 + o_P(1)) = A(n/k)(1 + o_P(1)),$$

in view of de Haan and Ferreira (2006, page 75). Second, using the same arguments as previously yields

$$\frac{1}{k}\sum_{j=0}^{k-1}\frac{1}{\rho}\left(\left(\frac{U(Y_{n-j:n})}{U(Y_{n-k:n})}\right)^{\xi+\rho} - \left(\frac{U(Y_{n-j:n})}{U(Y_{n-k:n})}\right)^{\xi}\right) \stackrel{d}{=} \frac{1}{k}\sum_{j=0}^{k-1}\frac{1}{\rho}((Y^*_j)^{\xi+\rho} - (Y^*_j)^{\xi}).$$

The laws of large numbers shows that this quantity converges in probability to $\tau(\xi, \rho)$ and therefore

$$T_{4,n} = \tau(\xi,\rho)A(n/k)(1 + o_P(1)). \tag{C.7}$$

From the definition of $T_{5,n}$, it follows that, for all $\varepsilon \in (0, 1 - \xi - \rho)$,

$$|T_{5,n}| \le A(n/k)(1 + o_P(1))\varepsilon\ \frac{1}{k}\sum_{j=0}^{k-1}\left(\frac{U(Y_{n-j:n})}{U(Y_{n-k:n})}\right)^{\xi+\rho+\epsilon}$$
$$\stackrel{d}{=} A(n/k)(1 + o_P(1))\varepsilon\ \frac{1}{k}\sum_{j=0}^{k-1}(Y^*_j)^{\xi+\rho+\epsilon}$$
$$= A(n/k)(1 + o_P(1))\varepsilon\mathbb{E}((Y^*_j)^{\xi+\rho+\epsilon})$$
$$= A(n/k)(1 + o_P(1))\frac{\varepsilon}{1-(\xi+\rho+\epsilon)}.$$

Letting $\varepsilon \to 0$ yields

$$T_{5,n} = o_P(A(n/k)). \tag{C.8}$$

Similarly, from the definition of $T_{5,n}$, it follows that, for all $\varepsilon \in (0, 1 - \xi - \rho)$,

$$|T_{6,n}| \le A^2(n/k)(1 + o_P(1))4(\varepsilon^2 + 1/\rho^2)\ \frac{1}{k}\sum_{j=0}^{k-1}\left(\frac{U(Y_{n-j:n})}{U(Y_{n-k:n})}\right)^{\xi}$$
$$\stackrel{d}{=} A^2(n/k)(1 + o_P(1))4(\varepsilon^2 + 1/\rho^2)\ \frac{1}{k}\sum_{j=0}^{k-1}(Y^*_j)^{\xi} \tag{C.9}$$

$$= A^2(n/k)(1 + o_P(1))4(\varepsilon^2 + 1/\rho^2)\mathbb{E}((Y^*_j)^{\xi})$$
$$= o_P(A(n/k)). \tag{C.10}$$

Collecting (C.5)–(C.10) proves the result.

C.4. Proofs of main results

Proof of Theorem 1. In view of Lemma 4, $T_{2,n} = o_P(1)$ and therefore Lemma 2 entails

$$\frac{1}{1-\hat{\xi}} - \frac{1}{1-\xi} = \left(T_{1,n} - \frac{1}{1-\xi} + \frac{\xi}{1-\xi}T_{2,n}\right)(1 + o_P(1))$$
$$= k^{-1/2}\sigma(\xi)\zeta(1 + o_P(1)) + \frac{\xi}{1-\xi}k^{\xi}\zeta_{\xi}(1 + o_P(1))$$
$$+ \tau(\xi,\rho)A(n/k)(1 + o_P(1)),$$

in view of Lemmas 4 and 5. Let $\theta = \min(1/2, -\xi)$. It follows that

$$k^{\theta}\frac{\hat{\xi} - \xi}{(1-\hat{\xi})(1-\xi)} = k^{\theta-1/2}\sigma(\xi)\zeta(1 + o_P(1)) + \frac{\xi}{1-\xi}k^{\theta+\xi}\zeta_{\xi}(1 + o_P(1))$$
$$+ \lambda\tau(\xi,\rho)(1 + o_P(1)),$$

under the assumption $k^{\theta}A(n/k) \to \lambda$ as $n \to \infty$. As a consequence, $\hat{\xi} \to P\xi$ and therefore

$$k^{\theta}(\hat{\xi} - \xi) = k^{\theta-1/2}\sigma(\xi)(1-\xi)^2\zeta(1 + o_P(1)) + k^{\theta+\xi}(1-\xi)\xi\zeta_{\xi}(1 + o_P(1))$$
$$+ \lambda(1-\xi)^2\tau(\xi,\rho)(1 + o_P(1)),$$

and the result is proved.

Proof of Corollary 1. Two cases arise. If $\xi < -1/2$ then $\theta = 1/2$ and thus $k^{1/2}(\hat{\xi}-\xi)$ is asymptotically Gaussian with mean $\lambda(1-\xi)^2\tau(\xi, \rho)$ and variance $\sigma^2(\xi)(1-\xi)^4$. Conversely, if $\xi > -1/2$, then $\theta = -\xi$ and $k^{-\xi}(\hat{\xi}-\xi)$ converges in distribution to $\lambda(1-\xi)^2\tau(\xi, \rho) + (1-\xi)\xi W(-1/\xi)$ where $W(-1/\xi)$ is the Weibull distribution with shape parameter $-1/\xi$.

C.5. Explanation for continuation in AUTO (Doedel, 1981)

In order to compute a family of solutions of a three-dimensional system

$$\mathbf{x}_\cdot = f(\mathbf{x}(t)) \tag{C.11}$$

we consider a function $\mathbf{u} : [0, 1] \mapsto \mathbb{R}^3$ satisfying a rescaled version of (C.11) given by the differential equation

$$\mathbf{u}_\cdot = Tf(\mathbf{u}(t)), \tag{C.12}$$

where f stands for the vector field defined by the system (4) and $T > 0$ is the integration time (also known as the "period") of an orbit segment of f. Note that in (C.12), the period T appears as an explicit parameter and the actual integration time over an orbit segment is always 1. Geometrically, the function $\mathbf{u}$ represents a unique orbit segment $\{\mathbf{u}(t) = (x(t), y(t), z(t)) \in \mathbb{R}^3 \mid 0 \le t \le 1\}$ provided that suitable boundary conditions are posed at one or both end points $\mathbf{u}(0)$ and $\mathbf{u}(1)$. In our case, we consider

$$\mathbf{u}(0) = (1, \mu, \nu), \tag{C.13}$$

where μ, ν are dummy parameters that determine the 'initial' coordinates y_0 and z_0, respectively, of a given solution.

The boundary value problem (C.12) and (C.13) defines a (μ, ν, T)-dependent family of orbit segments. For any fixed (μ, T) = (μ_0, T_0) we have a uniquely defined one-parameter family of orbit segments (parameterized by ν) with fixed integration time T_0 and fixed initial coordinates $x(0) = 1$, $y(0) = \mu_0$. In order to compute this ν-family by continuation in AUTO (Doedel, 1981; Doedel et al., 2010), we need to specify an initial orbit segment $\mathbf{u}_{\nu_0}$ that satisfies (C.12) and (C.13) for some fixed $\nu = \nu_0$. To this end, a possible choice is to take advantage of the continuous extension of (4) to the line $z = 0$ and consider the constant solution—i.e., a trivial orbit segment—$\mathbf{u}(t) \equiv (1, 0, 0)$ of (C.12) with $T = 0$; continuation in T for fixed $\mathbf{u}(0) = (1, 0, 0)$ up to $T = T_0$ yields the desired initial orbit segment $\mathbf{u}_0$ satisfying (C.12) and (C.13) for $\mu_0 = 0$ and $\nu_0 = 0$. A collection of orbits segments is then obtained by fixing $T = T_0$ and continuing $\mathbf{u}_0$ in μ up to a user-defined value; in our case, the stopping condition is $\mu = 1$. Finally, the desired family of orbit segments is obtained by allowing ν to vary while keeping $T = T_0$ and $\mu = 1$ fixed. In this way, each orbit segment in this family corresponds to a solution $\{\mathbf{x}(t) = (x(t), y(t), z(t)) \in \mathbb{R}^3 \mid 0 \le t \le T_0\}$ of (4) with initial condition $(x_0, y_0, z_0) = (1, 1, \nu)$.

References

Baker, M., 2016. Statisticians issue warning over misuse of *P* values. Nature 531 (March (7593)), 151, http://dx.doi.org/10.1038/nature.2016.19503.

Balakrishnan, N., Basu, A.P., 1996. The Exponential Distribution: Theory, Methods, and Applications. Gordon and Breach, New York.

Beran, J., Schell, D., Stehlík, M., 2014. The harmonic moment tail index estimator: asymptotic distribution and robustness. Ann. Inst. Stat. Math. 66 (1), 193–220.

Bingham, N.H., Goldie, C.M., Teugels, J.L., 1987. Regular Variation. Cambridge University Press.

Chan, E.Y., Liu, S., Hung, K.K., 1873. Typhoon Haiyan and beyond. Lancet 382, 2013.

Coles, S., 2001. An Introduction to Statistical Modeling of Extreme Values. Springer Series in Statistics. Springer, London, Berlin, Heidelberg.

Coumou, D., Rahmstorf, S., 2012. A decade of weather extremes. Nat. Clim. Change 2, 491–496.

de Haan, L., Ferreira, A., 2006. Extreme Value Theory: An Introduction. Springer-Verlag, New York.

Dekkers, A.L.M., de Haan, L., 1989 12. On the estimation of the extreme-value index and large quantile estimation. Ann. Stat. 17 (4), 1795–1832.

Doedel, E.J., Champneys, A.R., Dercole, F., Fairgrieve, T.F., Kuznetsov, Y., Oldeman, B.E., Paffenroth, R.C., Sandstede, B., Wang, X.J., Zhang, C.H., 2010. AUTO-07p: Continuation and Bifurcation Software for Ordinary Differential Equations. Department of Computer Science, Concordia University, Montreal, QC, Canada. Available from: http://cmvl.cs.concordia.ca/auto/

Doedel, E.J., 1981. AUTO: A program for the automatic bifurcation analysis of autonomous systems. Congr. Numer. 30, 265–284.

Doedel, E.J., 2007. Lecture notes on numerical analysis of nonlinear equations. In: Krauskopf, B., Osinga, H.M., Galán-Vioque, J. (Eds.), Numerical Continuation Methods for Dynamical Systems, Understanding Complex Systems. Springer-Verlag, New York, pp. 1–49.

Einmahl, J.H.J., Magnus, J.R., 2008. Records in athletics through extreme-value theory. J. Am. Stat. Assoc. 103 (484), 1382–1391.

Embrechts, P., Klüppelberg, C., Mikosch, T., 1987. Modelling Extremal Events for Insurance and Finance. Springer.

Fabián, Z., Stehlík, M., 2009. On robust and distribution sensitive hill like method. IFAS Res. Pap. Ser. 43 (4), 1–9. URL: http://www.jku.at/ifas/content/e108280/e146255/e146265/res43_steh.pdf.

Fabián, Z., 2001. Induced cores and their use in robust parametric estimation. Commun. Stat. Theory Methods 30, 537–556.

Falk, M., 1995. Some best parameter estimates for distributions with finite endpoint. Statistics 27 (1–2), 115–125.

Farrell, M.J., 1957. The measurement of productive efficiency. J. R. Stat. Soc. Ser. A: Gen. 120 (3), 253–290.

Furrer, R., Naveau, P., 2007. Probability weighted moments properties for small samples. Stat. Probab. Lett. 77 (2), 190–195.

Gascoin, S., Kinnard, C., Ponce, R., Lhermitte, S., MacDonell, S., Rabatel, A., 2011. Glacier contribution to streamflow in two headwaters of the Huasco river, dry Andes of Chile. Cryosphere 5 (4), 1099–1113.

Guckenheimer, J., Holmes, P., 1986. Nonlinear Oscillations, Dynamical Systems, and Bifurcations of Vector Fields, 2nd ed. Springer, New York.

Hasselblatt, B., Katok, A., 2003. A First Course in Dynamics: With a Panorama of Recent Developments. Cambridge University Press.

Hosking, J.R.M., Wallis, J.R., 1987. Parameter and quantile estimation for the generalized Pareto distribution. Technometrics 29 (3), 339–349.

Jordanova, P., Fabián, Z., Hermann, P., Střelec, L., Rivera, A., Girard, S., Torres, S., Stehlík, M., 2016. Weak properties and robustness of *t*-Hill estimators. Extremes 19, 591–626.

Kaser, G., 2003. A Manual for Monitoring the Mass Balance of Mountain Glaciers. Technical Documents in Hydrology. UNESCO-PHI, Paris. URL: http://globalcryospherewatch.org/cryonet/methods_docs/UNESCO_manual_glaciers_2003.pdf.

Klein Tank, A.M.G., Können, G.P., 2003. Trends in indices of daily temperature and precipitation extremes in Europe, 1946–99. J. Clim. 16, 3665–3680.

Leadbetter, R., Lindgren, G., Rootzén, H., 1983. Extremes and Related Properties of Random Sequences and Processes. Springer Series in Statistics. Springer-Verlag ISBN 9780387907314.

Müller, S., Chhay, H., 2011. Partially smooth tail-index estimation for small samples. Comput. Stat. 26 (3), 491–505.

Mayer, M., Molchanov, I., 2007. Limit theorems for the diameter of a random sample in the unit ball. Extremes 10 (3), 129–150, ISSN 1386-1999.

McCullagh, P., 2002. What is a statistical model? Ann. Stat. 30, 1225–1310, ISSN 1386-1999 (with discussion).

Penalva, H., Nunes, S., Neves, M.M., 2016. Extreme value analysis – a brief overview with an application to flow discharge rate data in a hydrometric station in the north of Portugal. REVSTAT 14 (2) .

Pickands III, J., 1975. Statistical inference using extreme order statistics. Ann. Stat. 3 (1), 119–131.

R Core Team, 2015. R: A Language and Environment for Statistical Computing. R Foundation for Statistical Computing, Vienna, Austria. URL: http://www.R-project.org.

Rabatel, A., Castebrunet, H., Favier, V., Nicholson, L., Kinnard, C., 2011. Glacier changes in the pascua-lama region, chilean andes (29s): recent mass balance and 50yr surface area variations. Cryosphere 5 (4), 1029–1041.

Sabolova, R., Seckarova, V., Dušek, J., Stehlík, M., 2015. Entropy based statistical inference for methane emissions released from wetland. Chemomet. Intell. Lab. Syst. 141, 125–133.

Sadovský, Z., Faško, P., Mikulová, K., Šťastný, P., 2007. Collection and analysis of climatic measurements for the assessment of snow loads on structures. Int. J. Reliab. Qual. Saf. Eng. 14 (6), 603–615.

Sadovský, Z., Faško, P., Mikulová, K., Pecho, J., Vojtek, M., 2009. Special features of the collection and analysis of snow loads. In: Martorell, S., Guedes Soares, C., Barnett, J. (Eds.), Safety, Reliability and Risk Analysis: Theory, Methods and Applications. ESREL 2008 Valencia, vol. 2. Taylor & Francis Group, London, pp. 1671–1675.

Sadovský, Z., Faško, P., Mikulová, K., Pecho, J., 2010. Assessment of accidental snow loads for the design of structures. In: Ale, B.J.M., Papazoglou, I.A., Zio, E. (Eds.), Reliability, Risk and Safety – Back to the Future: ESREL 2010. Taylor & Francis Group, London, ISBN 978-0-415-60427-7, pp. 1549–1552.

Sadovský, Z., Faško, P., Mikulová, K., Pecho, J., 2012. Exceptional snowfalls and the assessment of accidental snow loads for structural design. Cold Regions Sci. Technol. 72, 17–22.

Sanpaolesi, L., et al., 1998. Phase 1 Final Report to the European Commission, Scientific Support Activity in the Field of Structural Stability of Civil Engineering Works: Snow Loads. Dept. of Structural Engineering, University of Pisa.

Smith, R.L., 1985. Maximum likelihood estimation in a class of nonregular cases. Biometrika 72, 67–90.
Stehlík, M., Potocký, R., Waldl, H., Fabián, Z., 2010. On the favourable estimation of fitting heavy tailed data. Comput. Stat. 25, 485–503.
Stehlík, M., Sadovský, Z., Jordanova, P., 2015. Statistical analysis related to exceptional snow loads. Appl. Math. Inf. Sci. 9 (1L), 19–27.
Stehlík, M., Dušek, J., Kiseľák, J., 2016. Missing chaos in global climate change data interpreting? Ecol. Complex. 25, 53–59.
Stehlík, M., 2008. Homogeneity and scale testing of generalized gamma distribution. Reliab. Eng. Syst. Saf. 93, 1809–1813.
Zhou, C., 2009. Existence and consistency of the maximum likelihood estimator for the extreme value index. J. Multivar. Anal. 100 (4), 794–815.
Zhou, C., 2010. The extent of the maximum likelihood estimator for the extreme value index. J. Multivar. Anal. 101 (4), 971–983.